STARS

Electronic Theses and Dissertations, 2020-

2022

Biomimetic Design, Modeling, and Adaptive Control of Robotic Gripper for Optimal Grasping

Mushtaq Al-Mohammed
University of Central Florida

Showcase of Text, Archives, Research & Scholarship

BIOMIMETIC DESIGN, MODELING,AND ADAPTIVE CONTROL OF ROBOTIC GRIPPER
FOR OPTIMAL GRASPING

by

MUSHTAQ TALIB AL-MOHAMMED
B.S. University of Technology, Iraq, 2001
M.S. University of Technology, Iraq, 2009
M.S. University of Central Florida, 2018

A dissertation submitted in partial fulfilment of the requirements
for the degree of Doctor of Philosophy
in the Department of Electrical and Computer Engineering
in the College of Engineering and Computer Science
at the University of Central Florida
Orlando,Florida

Spring Term
2022

Major Professor: Aman Behal

ABSTRACT

Grasping is an essential skill for almost every assistive robot. Variations in shape and/or weight of different objects involved in Activities of Daily Living (ADL) lead to complications, especially, when the robot is trying to grip novel objects for which it has no prior information –too much force will deform or crush the object while too little force will lead to slipping and possibly dropped objects. Thus, successful grasping requires the gripper to immobilize an object with the minimal force. In Chapter 2, we present the design, analysis, and experimental implementation of an adaptive control to facilitate 1-click grasping of novel objects by a robotic gripper. Motivated by a desire to obtain a reduced-order controller, a previously developed grasp model is reparameterized to design an adaptive backstepping controller. A Lyapunov-based analysis is utilized to show asymptotic convergence of the object slip velocity to the origin. Furthermore, the analysis shows that the closed-loop controller is able to estimate the minimal steady-state force required to grasp the object. Simulation and experiment results both show that the object is immobilized within the gripper without any significant deformation. Also, in Chapter 3 we present the design and implementation of an algorithm, equipped with a switched adaptive controller, for grasping unknown objects using a robot gripper. A Lyapunov-based analysis demonstrates that the switching controller is indeed asymptotically stable with both the translational and rotational slip velocities converging to the origin. Experimental results using a novel sensorized gripper prototype and objects of different sizes, shapes, and weights show that the proposed algorithm not only ensures prevention of slippage of the grasped objects, but it is also able to apply the minimal force needed to safely grasp these objects without causing excessive deformation.

In Chapter 4, the Pearson and Spearman correlation tests are employed to capture the joint probability distribution of human variables related to human-robot interaction using experiment data obtained from 93 individuals. The findings show that some human factors are jointly distributed

within the same group as: (spatial visualization (SpV), spatial orientation (SpO), and visual perception (VP)), (gross dexterity (GD) and fine dexterity (FD)) and (visual acuity WV and SV), while the Reaction Time (RT), working memory (WM), depth perception (DP) are related insignificantly. Furthermore, we present Principal Components Analysis (PCA) of human factors. By using Varimax Rotation matrix to gain obvious interpretations, it confirms the same observations about the interdependencies between the human factors.

To my parents, my wife, and my daughters ...

ACKNOWLEDGMENTS

I would like to express my deepest and sincere gratitude to my PhD advisor, Dr. Aman Behal, for his enormous amount of guidance and support throughout my PhD journey.

Also, I want to thank the rest of my dissertation committee members: Dr. Janan Smither, Dr. Gita Sukthankar, Dr. Michael Haralambous, and Dr. Yaser Fallah for their time and constructive advice and comments. I also want to acknowledge the Ministry of Higher Education and Scientific Research and Al-Nahrain University in my home country, Iraq, for supporting me to pursue my PhD. I am grateful to my former lab-mates in the UCF Assistive Robotics Laboratory specifically Nicholas Paperno, Zhangchi Ding, and Robson Adem for their help and collaboration.

I am also thankful to all my friends and relatives for their support. I would like to say a special thank you to my beloved wife, Oras, and my daughters, Yaqeen, Zahraa, Rawan, and Layan, for their continuous encouragement, patience, and support. Finally, my sincere gratitude goes to whom I owe everything - my big family: my beloved mother, my brothers and sisters, and to the soul of my father.

Again, thank you all!

TABLE OF CONTENTS

LIST OF FIGURES

LIST OF TABLES

CHAPTER 1: INTRODUCTION

One of the biggest endeavors in robotics is to endow robots with the ability to grasp a variety of objects with precision and accuracy via direct interaction with its environment similar to how human hands are utilized in daily activities. To this end, for decades, modern robotic arms have incorporated robotic grippers of different sizes and types to accomplish heterogeneous tasks in broad application areas including industrial, medical, collaborative, and assistive technologies. Most robots (JACO, MICO, iARM, PR2, Baxter, NAO, etc.) possess two-finger and in some cases three-finger grippers to satisfy the most important conditions of grasping objects, namely, form closure and force closure. In addition, robotic grippers ought to be controlled to optimize the force applied by the finger-gripper so as to not cause slippage and/or deformation of objects, which in many applications is undesirable. Furthermore, this pursuit faces a significant challenge due to the complexity that arises from a large diversity of objects that a robot is required to grasp. The complexity intensifies considerably as the order of the structure of the environment and pre-existing knowledge of objects' shape and size decreases. Grasping an object with insufficient force may cause a failure in picking the object appropriately or cause it to slip during manipulation of the robot to place the grasped object elsewhere. On the other hand, grasping too firmly can unintentionally crush or damage objects – this may have economic or safety implications. Therefore, the ability to adaptively control robotic grippers in real-time to apply minimal force that prevents slippage as well as deformation of grasped objects is indispensable for certain tasks where delicate objects are being handled (*e.g.,* assistive robots performing ADL tasks).

Previous papers have proposed slip avoidance techniques to solve the problem at hand with slip detecting sensors ranging from biomimetic to optical-mechanical sensors. These approaches can be grouped into optical-sensor-based, pressure/force-based, and vibration-based. In [1], researchers studied the efficacy of the use of optical sensors for a variety of textures. In [2], a closed-loop

controller, equipped with an optical sensor for slip detection, was used to tune the grasping force. However, the study mentioned neither if the grasped force avoids deformation of objects nor if the controller can be used beyond the only one object they tested for. In [3], upon detection of slip, via an optical-mechanical tactile sensor, objects were grasped by a preset amount of force to prevent additional slip and ensure fine finger-force control. In [4] and [5], following a slip event, detected by tracking the rate of change of force from static conditions against a preset threshold, the gripper applies an additional grasping force that is established prior to slip detection. In [6], a pressure conductive rubber was used to construct a slip sensor to apply a gripping force proportional to the slip signal. In [7], a sliding mode controller was designed to approximate the grasping force after calculating slip based on the high frequency vibration of the shear force and its derivative; however, the ISMSP controller is slow to converge and only accounts for translational slipping. In [8], researchers used a biomimetic tactile sensor in order to establish force estimation together with slip detection and classification. They used machine learning techniques to map slip signals, detected by the change in the tangential force and slip-related micro-vibrations from the sensor, to force. In addition, a gripper force was controlled by estimating the friction coefficient. In [9]-[11], minimum force object immobilization controllers are considered using 6-axis F/T sensors and no motion sensors but they do require initial object exploration as well as offline estimation of the translational and rotational stiffnesses of the sensor pad which is an implicit way to generate object motion estimates through an admittance formulation. In [12], an algorithm is described that is intuitive but suffers from the issue of having to require a large number of parameters including object stiffness. An empirical approach in [13] proposes a learning-based approach for slip prediction but suffers from failure to compensate for rotational slip. A recent work in [14] provides a novel control formulation but does not offer stability guarantees. Machine-learning approaches to tactile force and object dynamics inferencing have been reported in [15] and [16]. Although the aforementioned methods provided solid proposals, none of them meets the overall goal of building a real-time system theoretic adaptive system with stability guarantees that can be implemented

out of the box for preventing slippage of never before seen objects while also minimizing grasped object deformation.

In our initial work in [18], an open-loop force flatness detection-based adaptive grasping algorithm was implemented to grasp a large set of novel objects. While this technique works for some objects, it is not successful for "soft and compressible" objects like plastic and Styrofoam cups which do not provide any functional flatness profile before deformation. Prompted by this, in [19] we implemented a closed-loop adaptive algorithm which effectively grasped an arbitrary wide set of objects with minimal grasping force after slip has been detected. Motivated by our desire to design a reduced-order controller, in Chapter 2 [20], we propose a reparameterization for the system model developed in [19]. This facilitates the design of an adaptive controller that guarantees stability and convergence of the object slip velocity. Specifically, using a simple linearly parameterizable model for the interaction between a robotic gripper and an arbitrary object, we design an adaptive backstepping controller that relies on measurements of the object-gripper interaction force and object slip velocity. A Lyapunov-based stability analysis is utilized to show asymptotic convergence of the object slip velocity to the origin. The analysis also shows that the closed-loop controller is able to estimate the minimal steady-state force required to grasp the object. The main advantage of this work over its predecessors is the reduced order and, thereby, lower computational complexity of the controller.

To extend our previous designs so as to be able to avoid both linear and rotational slippage, in Chapter 3, a new model is derived and thus a corresponding modification of adaptive control based on switching between translational and rotational motion-based controllers is proposed [21] . Moreover, in the past work the controller design relied on measurements of the object-gripper interaction force and object linear slip velocity. In order to estimate the angular slip velocity of the grasped object, we redesigned our sensorized robotic gripper prototype in [19] to incorporate a single force sensing resistor (FSR) and a stereo laser-based optical slip sensor set. The main contribution of this

work, in addition to the novel sensorized gripper prototype design and gripper-object interaction modeling, is the novel real-time algorithm that can adaptively grasp objects independent of their geometry, texture, and weight. Furthermore, the algorithm guarantees the application of minimal grasping force, to minimize object deformation as long as there is pure rotational or translational motion. When there exists a combination of motions and switching is activated, no guarantees can be provided; however, extensive experimental results show that the force applied is close to the minimal required for immobilization.

Until this point, we have studied how to model gripper object interaction and adapted for it to design control based on different object shape, gripper type, and friction between gripper/ object, etc. This adaptation is needed to get optimal gripper force. Similarly, optimal interaction is needed between human and robot based on individual differences between various users. In order to facilitate engagement with a robot, Human-Robot Interaction (HRI) needs to be modeled and incorporated into the interface such that the robot is responsive to the individual needs of the particular user. Since the advent of robot teleoperation, researchers have been studying many characteristics of a person's being (also known as human factors) to identify which ones have an influence on performance. The majority of research looking at human factors that impact user's performance aim to find techniques to identify potential skilled operators. Also, by identifying which factors are most relevant, the performance of individuals can be improved by enhancing these factors through training and/or adapting human robot interface. According to Lathan and Tracy, individuals with better spatial perception abilities produced fewer mistakes when managing a teleoperated robotic system [22]. Gomer and Pagano [23] as well as Long and co-researchers [24]-[25] went even farther, examining the distinct components of spatial skills to see how they related to user performance. NASA has conducted several studies to identify how to assess potential manipulator operators for the shuttle based on spatial abilities [26]-[28]. Wang *et al.* reported on the use of a teleoperation system to predict a person's performance based on spatial abilities in a rendezvous and docking

missions [27]. Paperno *et al.* recently conducted a major user research to model significant differences in order to anticipate a user's performance when using a robotic manipulator to execute pick-and-place/object retrieval tasks [29]. Several human factors were discovered to be significant determinants of task completion speed, command quantity, and command input rate. Motivated by the findings of the study in [29], we propose a putative model for joint probability distribution of human factors utilizing Principal Components Analysis (PCA) as well as Pearson and correlation tests detailed in Chapter 4.

CHAPTER 2: AN ADAPTIVE CONTROL BASED APPROACH FOR GRIPPING NOVEL OBJECTS WITH MINIMAL GRASPING FORCE

M. Al-Mohammed and Z. Ding and P. Liu and A. Behal "An Adaptive Control Based Approach for Gripping Novel Objects with Minimal Grasping Force," *IEEE 14th International Conference on Control and Automation (ICCA) Anchorage, AK, 2018,*, pp.1040-1045.

Problem Statement and Modeling

Using gripper velocity as the control input and the applied grasping force as well as the object slip velocity as the measurements, the goal of this research is to drive a robot gripper to successfully grasp a novel object with minimal grasping force. The geometry, weight, and texture of the object are assumed to be unknown. Figure 2.1 shows the gripper fingers grabbing an arbitrary object which is acted upon by a constant disturbance force W, applied gripper force F_a, and frictional force $F_f = \mu F_a$ where μ is the coefficient of friction between the gripper and the object such that the dynamics of the slip velocity $v(t)$ can be written as

$$m\dot{v} = W - \mu F_a. \tag{2.1}$$

which can be reparameterized as follows

$$a\dot{v} = b - F_a \tag{2.2}$$
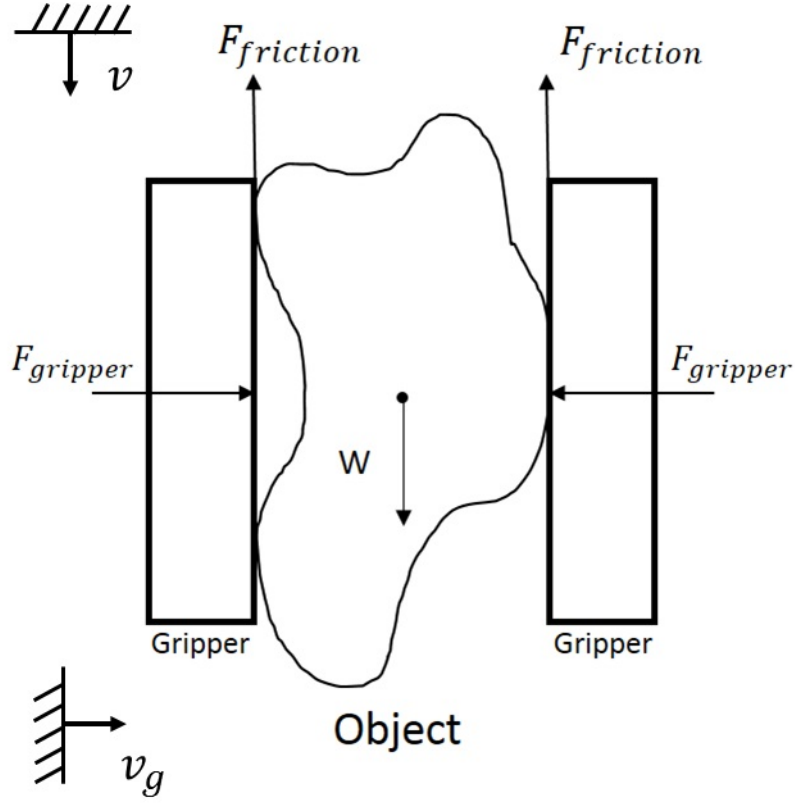
Figure 2.1: The Free Body Diagram for Gripper Object Interaction

where $a = m/\mu$ and $b = W/\mu$. Since it is not possible to directly control and apply the gripper force $F_a(t)$, we model the incremental displacement $x_g(t)$ of the gripper as proportional to the applied force such that

$$F_a \propto x_g \tag{2.3}$$

the time derivative of which can be related to the control input signal, the gripper velocity $v_g(t)$, as follows

$$\dot{F}_a = \kappa v_g \tag{2.4}$$

Thus, (2.2) and (2.4) represent the overall system dynamics. Here, in deference to our problem statement above, $a, b,$ and κ are assumed to be unknown parameters of which we will adapt for b and κ during the control design process.

Control Design and Stability Analysis

In this section, an adaptive backstepping approach will be utilized based on the slip and force measurements from the finger sensor. Based on the backstepping approach, we can design a desired gripper force as

$$F_d = \hat{b} + k_1 v \tag{2.5}$$

where k_1 is a positive control gain and $\hat{b}(t)$ is a parameter estimate that is yet to be designed. Now, by adding and subtracting $F_d(t)$ to (2.2), we can get

$$a\dot{v} = \tilde{b} - F_e - k_1 v \tag{2.6}$$

where $F_e(t)$ is an auxiliary error variable defined as

$$F_e \equiv F_a - F_d, \tag{2.7}$$

while $\tilde{b}$ is a parameter estimation error defined as follows

$$\tilde{b} \equiv b - \hat{b}. \tag{2.8}$$

To motivate the design for an adaptive parameter estimator, we define a positive-definite function $V_0(t)$ as follows

$$V_0 = \frac{1}{2}av^2 + \frac{1}{2}\gamma_1^{-1}\tilde{b}^2 \tag{2.9}$$

8

where a and γ_1 are positive constants. After differentiating (2.9) along the trajectory of (2.6) and rearranging terms, one can obtain

$$\dot{V}_0 = -k_1 v^2 - F_e v + (v - \gamma_1^{-1}\dot{\hat{b}})\tilde{b} \tag{2.10}$$

Based on the parenthesized term in (2.10), we design an adaptive estimator for $\hat{b}(t)$ as follows

$$\dot{\hat{b}} = \gamma_1 v \tag{2.11}$$

By substituting (2.11) into (2.10), we obtain

$$\dot{V}_0 = -k_1 v^2 - F_e v. \tag{2.12}$$

To complete the design, we can time differentiate (2.7) to obtain the dynamics of $F_e(t)$ as follows

$$\dot{F}_e = \kappa v_g - \gamma_1 v - Y\theta \tag{2.13}$$

where $Y(t) \equiv [k_1 \quad -k_1 F_a(t)]$ is a measurable regression vector, $\theta \equiv [\frac{b}{a} \quad \frac{1}{a}]^T$ is an unknown parameter vector, and we have utilized (2.2) and (2.11) to substitute for $\dot{v}(t)$ and $\dot{\hat{b}}(t)$, respectively. Motivated by the structure of (2.13), we can design $v_g(t)$ as follows

$$v_g = \hat{\kappa}^{-1}(v - k_2 F_e + \dot{\hat{b}} + Y\hat{\theta}) \tag{2.14}$$

where k_2 is a positive control gain, while $\hat{\kappa}(t)$ and $\hat{\theta}(t)$ are parameter estimates which are yet to be designed. After substituting (2.14) into (2.13) and rearranging the terms, we obtain

$$\dot{F}_e = v - k_2 F_e - Y\tilde{\theta} + \tilde{\kappa}\hat{\kappa}^{-1}(v - k_2 F_e + \dot{\hat{b}} + Y\hat{\theta}) \tag{2.15}$$

9

where $\tilde{\kappa}\left(t\right), \tilde{\theta}\left(t\right)$ are parameter estimation errors defined as follows

$$
\begin{aligned}
\tilde{\kappa} &\equiv \kappa - \hat{\kappa} \\
\tilde{\theta} &\equiv \theta - \hat{\theta}
\end{aligned}
\tag{2.16}
$$

To analyze the stability of the overall system and design the adaptive parameter estimation for $\hat{\kappa}\left(t\right)$ and $\hat{\theta}(t)$, we define another positive-definite function $V(t)$ as follows

$$
V = V_0 + \frac{1}{2}F_e^2 + \frac{1}{2}\gamma_2^{-1}\tilde{\kappa}^2 + \frac{1}{2}\gamma_3^{-1}\tilde{\theta}^T\tilde{\theta}
\tag{2.17}
$$

where γ_2 and γ_3 are positive constants, while $V_0(t)$ has been previously defined in (2.9). By time differentiating (2.17) along (2.12) and (2.15) and rearranging the terms, we obtain

$$
\begin{aligned}
\dot{V} = \quad & -k_1 v^2 - k_2 F_e^2 + \tilde{\theta}^T\left[-Y^T F_e - \gamma_3^{-1}\dot{\hat{\theta}}\right] \\
& -\tilde{\kappa}\left[\gamma_2^{-1}\dot{\hat{\kappa}} - \hat{\kappa}^{-1}(v - k_2 F_e + \dot{\hat{b}} + Y\hat{\theta})F_e\right]
\end{aligned}
\tag{2.18}
$$

Motivated by the structure of the bracketed terms in (2.18), the adaptive update laws for $\hat{\kappa}\left(t\right)$ and $\hat{\theta}(t)$ can be designed as follows

$$
\begin{aligned}
\dot{\hat{\kappa}} &= \gamma_2\hat{\kappa}^{-1}(v - k_2 F_e + \dot{\hat{b}} + Y\hat{\theta})F_e \tag{2.19} \\
\dot{\hat{\theta}} &= -\gamma_3 Y^T F_e \tag{2.20}
\end{aligned}
$$

Substituting (2.19) and (2.20) into (2.18) yields a negative semi-definite expression for $\dot{V}(t)$ as follows

$$
\dot{V} = -k_1 v^2 - k_2 F_e^2 \quad \leq 0
\tag{2.21}
$$

It is clear to see from (2.17) and (2.21) that $v\left(t\right), F_e\left(t\right) \in \mathcal{L}_2 \cap \mathcal{L}_\infty$ while $\hat{b}\left(t\right), \hat{\kappa}\left(t\right), \hat{\theta}\left(t\right) \in \mathcal{L}_\infty$. Based on previous assertions, it is also clear to see from (2.6) and (2.15) that $\dot{v}\left(t\right), \dot{F}_e\left(t\right) \in \mathcal{L}_\infty$.

Thus, one can utilize Barbalat's Lemma [37][38] to prove that $\lim_{t \to \infty} v(t), F_e(t) = 0$. Now, based on (2.6), it is clear to see that $\lim_{t \to \infty} \tilde{b}(t) = 0$. From the aforementioned facts and (2.5), it is clear to see that $F_a = F_d = W/\mu$ in the limit which implies that the object gets immobilized in the gripper with minimal grasping force.

Remark1: A block diagram of the complete control design given by (2.5), (2.11), (2.14), (2.19), and (2.20) is shown in Figure 2.2
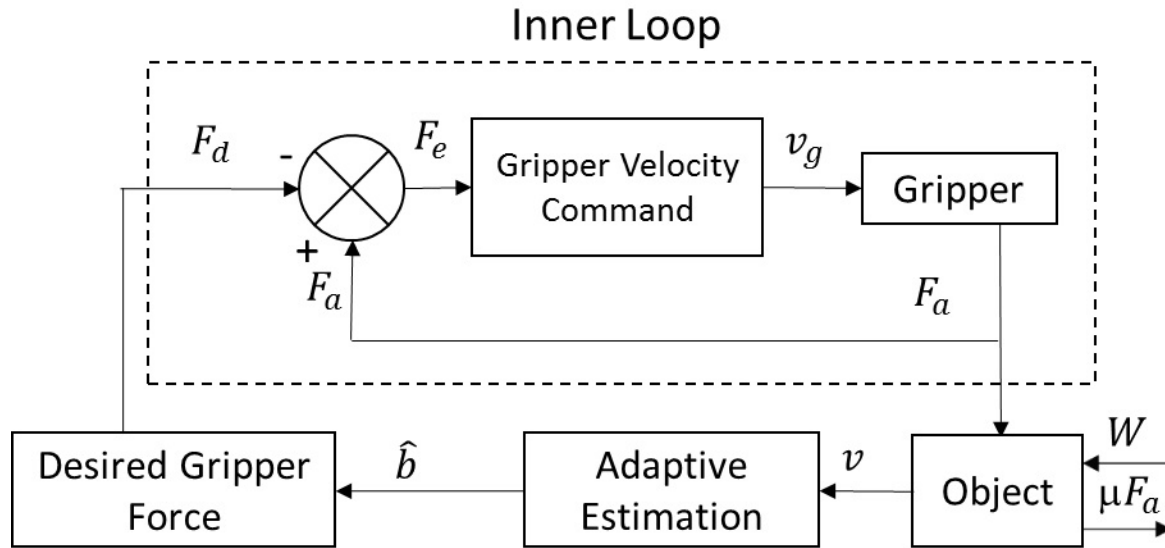
Figure 2.2: Block diagram of the full adaptive grasping controller.

Implementation

Experimental Setup

The testbed for the proposed adaptive algorithm is the UCF-MANUS platform [36] which has a gripper embedded with a force sensing resistor (FSR) and a laser-based slip sensor. The gripper

11

setup is shown in Figure 2.3. Details of the Gripper Prototype Assembly are available in [19]. We utilized a half-filled and a fully-filled water bottle as test objects for the experiments.
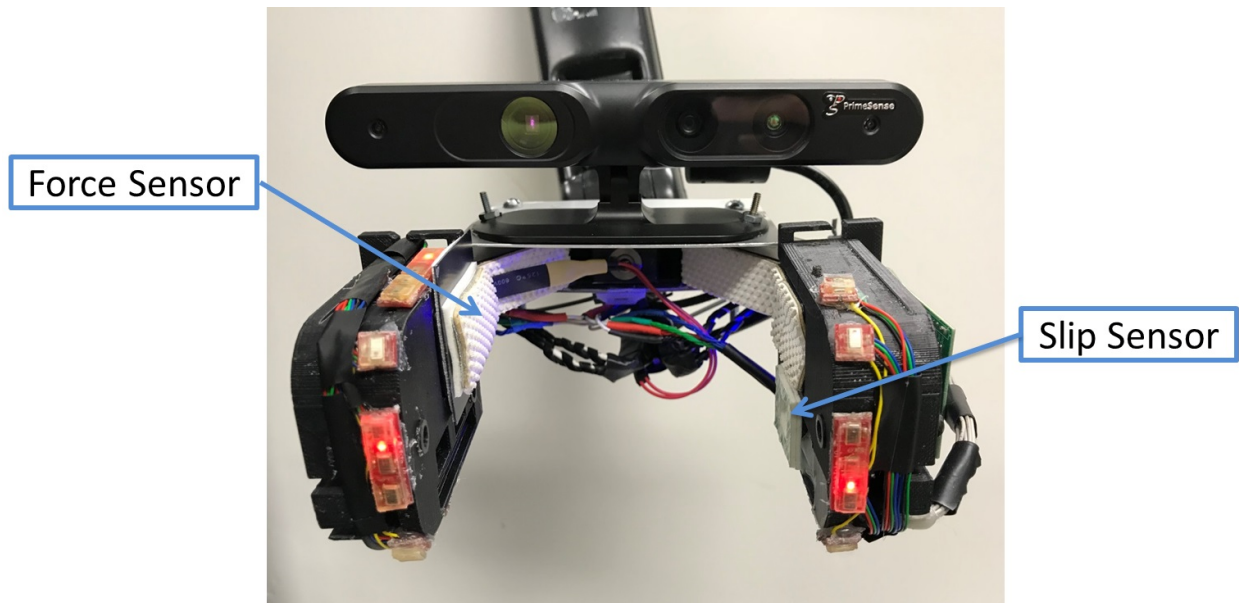
Figure 2.3: Assembled gripper setup

Experimental Protocol

There are two steps in the process for testing the proposed closed-loop adaptive algorithm. The initial step is to grasp the object with the smallest detectable force. At this time, the gripper tries to lift the object from its resting surface. If the initial grasp force is not enough to lift the object, slipping will occur at which time the adaptive regrasping controller will start to adjust the grasping force. Figure 2.4 shows the progression of steps involved in initial grasping and adaptive regrasping as needed.
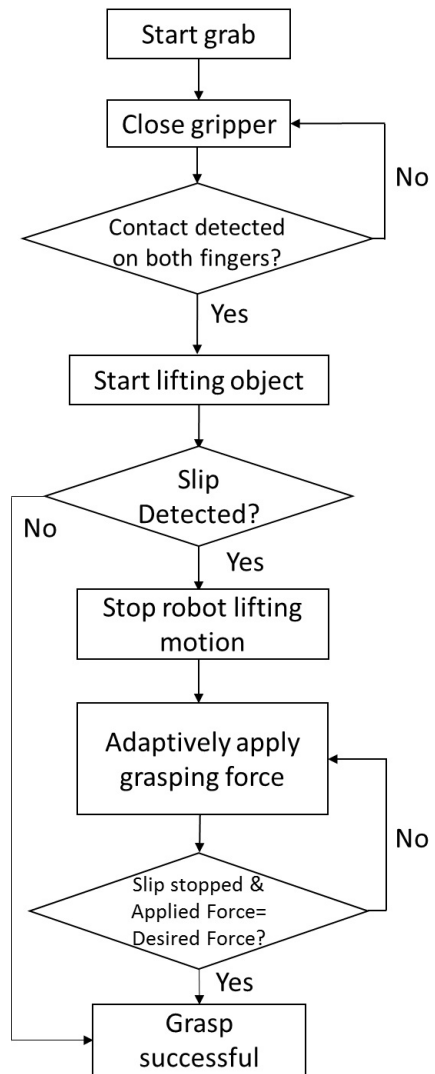
Figure 2.4: Flowchart of the proposed grasping algorithm

Initial Grasping

The details of the initial grasping are as follows. Since the gripper is asymmetric in terms of mea-

surements (*i.e.,* force sensing on one side and slip sensing on the other), both the slip and force

sensors are employed to ensure that both fingers are touching the object. It was determined experi-

mentally that a force measurement of greater than $0.5N$ combined with a detected slip velocity of

at least $0.1mm/s$ ensures a bilateral contact condition. Once contact is detected on both sides, the initial grasping phase is considered to be complete.

Adaptive Regrasping

Object will slip between the gripper fingers when the initial grasping force is not sufficient to counter gravitational force. Then the adaptive regrasping controller will be activated to stop the slipping. To simplify the implementation of the controller designed in Section 2, we utilize a timescale separation assumption to divide the controller into an outer loop and an inner loop as shown in Figure 2.5. The outer loop computes the desired gripper force $F_d(t)$ while the inner loop utilizes the gripper velocity command $v_g(t)$ to zero out the force error between the actual force $F_a(t)$ and the desired force $F_d(t)$. The simplified nested adaptive controller can be described mathematically as follows

$$F_d = \hat{b} + k_1 v$$
$$\dot{\hat{b}} = \gamma_1 v \tag{2.22}$$
$$v_g = -k_2 (F_a - F_d)$$
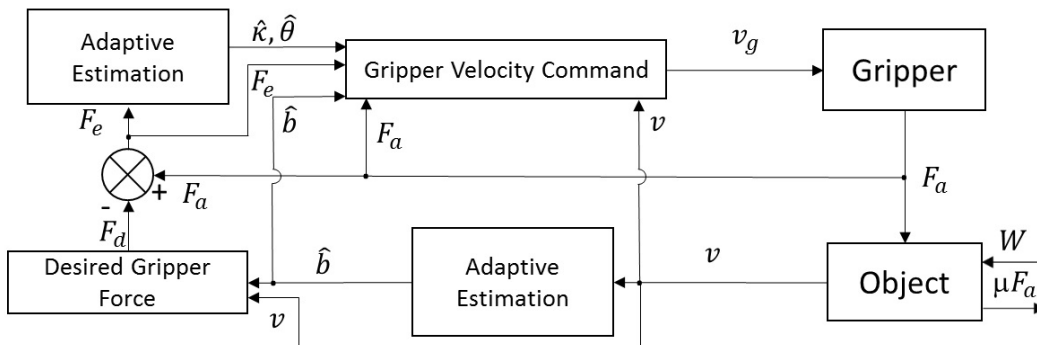
Figure 2.5: Block diagram of the simplified nested adaptive controller used for implementation

14

Table 2.1: Model Parameters For Both Approaches

$m = 0.5kg$	$g = 9.8m/s^2$
$\mu = 1.5$	$\kappa = 15N/cm$
$Fa(0) = 2N$	

Table 2.2: Controller Parameters for simulating the proposed approach

$k_1 = 8$	$k_2 = 20$
$\gamma_1 = 60$	$\gamma_2 = 2$
$\gamma_3 = 2$	$\hat{b}(0) = 2$
$\hat{\theta}(0) = [\ 1\quad 0.5\ ]^T$	

Remark2:We note here that the simplified controller design shown above in (2.22) is of lower order than the simplified adaptive controller implemented in [19].

Results

Simulation Results

In this section, the proposed adaptive controller and the original adaptive controller presented in [19] are simulated for the object-gripper interaction model stated in Section 2. A simple object was modeled by a certain weight and a friction coefficient. The model parameters utilized during numerical simulation are shown in Table 2.1. Table 2.2 shows the controller parameters for the proposed approach while Table 2.3 shows the controller parameters for the approach proposed in [19].

The simulation results using the proposed approach can be seen in Figure 2.7 where it can be seen that the object gets immobilized in 0.5s. The estimated value of b converges to the true minimal

15

Table 2.3: Controller Parameters for simulating the approach proposed in [19]

$k_1 = 12$	$k_2 = 20$
$\gamma_1 = 30$	$\gamma_2 = 5$
$\gamma_3 = 2$	$\gamma_4 = 2$
$\hat{W}(0) = 3$	$\hat{\mu}(0) = 1.5$
$\hat{\theta}(0) = [\ 1 \quad 0.5\ ]^T$	

Table 2.4: Experiment Controller Parameters

$k_1 = 600$	$k_2 = 5$
$\gamma_1 = 700$	$\hat{b}(0) = 1.4N$

grasping force which is 3.26N. We can also easily notice that the applied force tracks the desired force very well. During the entirety of the regrasping process, the object only slipped by 2.1cm while the peak velocity of the gripper is seen to be 2.3 cm/s which is an achievable speed for most grippers. The results for the design proposed in [19] can be seen in Figure 2.6. It can seen that the object gets immobilized in 0.6s. The estimates for the parameters μ and W are 1.128 and 3.684 which is clearly not close to the true value. However, the ratio of these parameter estimates is equal to the ratio for the actual parameters which shows that minimal gripping force is utilized. The gripper controller also drives the gripper to track the desired force perfectly. During the entirety of the regrasping process, the object slips as low as 2.28cm which is 1.8mm longer than proposed approach. The peak velocity of the gripper is 2.0 cm/s which is 0.3cm/s lower than the proposed approach. Thus, it is clear to see that both approaches obtain similar performance while the proposed approach has less complexity than the previous approach in [19].
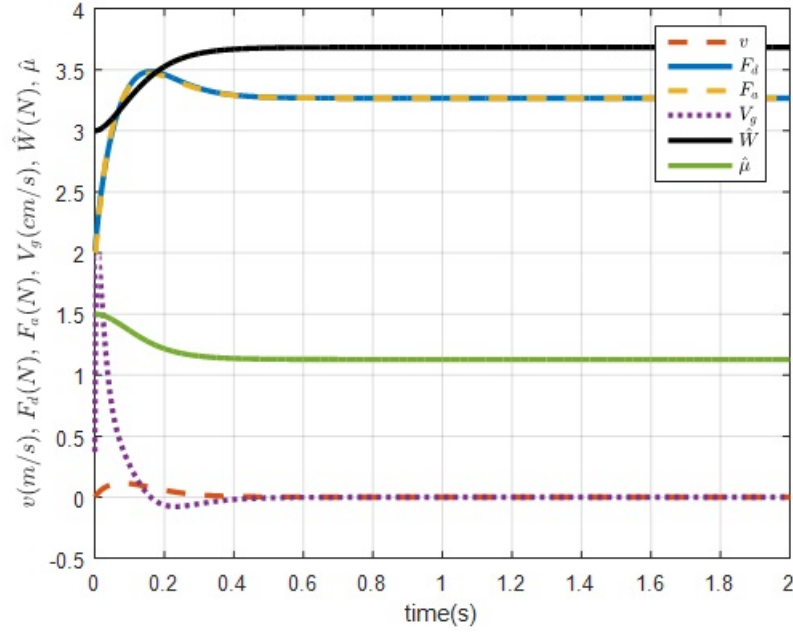
Figure 2.6: Simulation results for the proposed approach

Table 2.5: Actual and Estimated Parameter Values

	Parameters	
	Half-filled Bottle	Fully-filled Bottle
Value	F_a	F_a
Actual	1.8N	3.1N
Estimated	2.0N	3.1N

Experimental Results

The experimental results for a half-filled and a fully-filled bottle are presented in Figure 2.8 and Figure 2.9, respectively. The controller parameters for the simplified adaptive design of (2.22) are shown in Table 2.4. In Figure 2.8, the half-filled bottle is initially grasped with a force of $1.4N$. However, slipping occurs during lifting at which time the adaptive controller gets activated to immobilize the object. The final estimated grasping force is $2.0N$. Slippage is also seen to

17
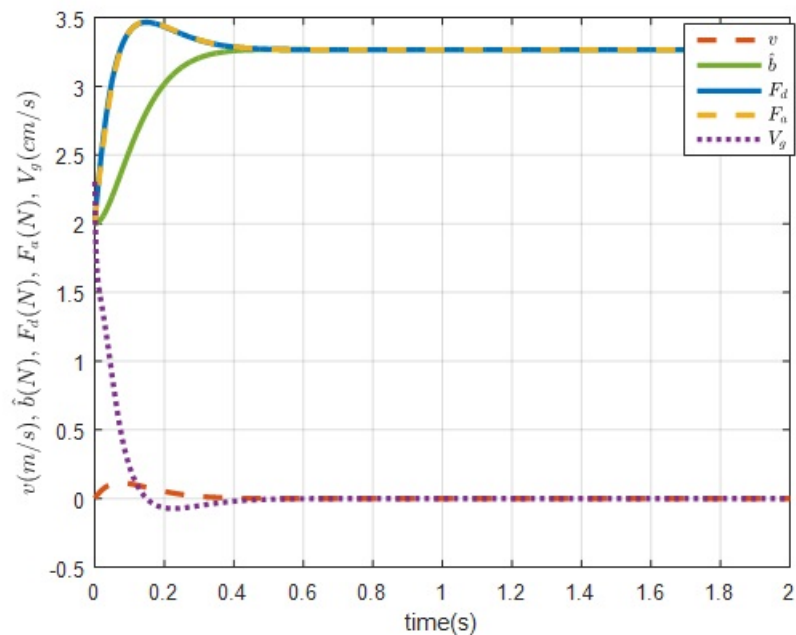
Figure 2.7: Simulation results for the approach proposed in [19]

occur for the full-filled bottle as shown in Figure 2.9. The final estimated grasping force is $3.1N$.

The comparison between the estimated and the true minimal grasping force is listed in Table 2.5.

From the table, we can easily see that the estimated value for the fully-filled bottle is equal to the

minimal grasping force, while the estimated value for the half-filled bottle is only $0.2N$ larger than

the minimal grasping force.
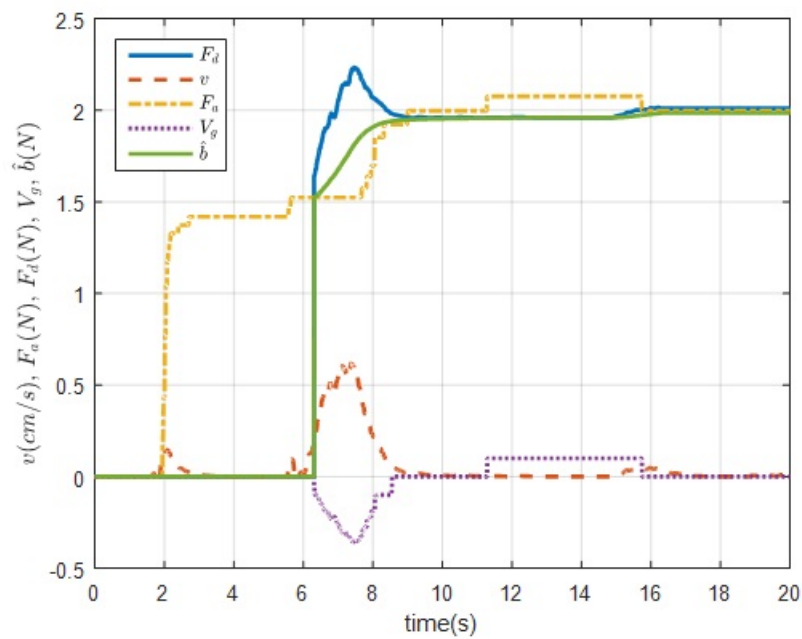
Figure 2.8: Slip detection and regrasping of half-filled water bottle. Initial grasping stage lasts between t = 0s and t = 5.5s using an initial grasp force of 1.41N. Robot starts lifting the bottle at t = 5.5s and the algorithm detects slipping at t = 6.3s at which time the proposed closed-loop adaptive algorithm activates to stop slipping using final grasping force of 2.0N
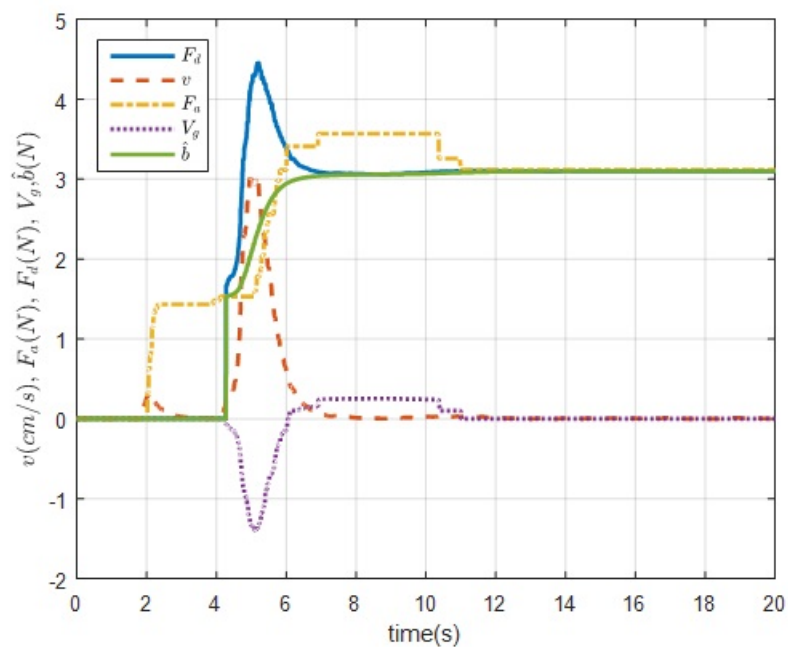
Figure 2.9: Slip detection and regrasping of fully-filled water bottle. Initial grasping stage lasts between t = 0s and t = 3.9s using an initial grasp force of 1.43N. Robot starts lifting the bottle and slipping is detected at t = 4.27s at which time the proposed closed-loop adaptive algorithm activates to stop slipping using final grasping force of 3.1N.

CHAPTER 3: A SWITCHED ADAPTIVE CONTROLLER FOR ROBOTIC GRIPPING OF NOVEL OBJECTS WITH MINIMAL FORCE

M. Al-Mohammed, R. Adem, and A. Behal "A Switched Adaptive Controller for Robotic Gripping of Novel Objects with Minimal Force," *IEEE Transactions on Control Systems Technology*, accepted, 2022.

Problem Statement and Modeling

The aim of this research is to design an algorithm to adaptively control robotic grippers in real-time to apply minimal force that prevents slippage while respecting the critical constraint on deformation of grasped objects. In order to achieve this objective, the gripper velocity will be utilized as the control input while the slip velocities (*i.e.,* linear and angular) and applied grasping force will be the available measurements for the controller. Figure 3.1 shows a free body diagram for an object undergoing rotational and translation motions. The gripper finger is acted upon by the torque caused by mg, the applied force F_a, frictional force μF_a, and the rotational friction force βF_a, where μ and β are the coefficients of linear and rotational friction between the gripper and the object. The dynamics of this system can be derived using a Lagrangian formulation as given below.

The total kinetic energy T can be written as

$$T = \frac{1}{2}I\dot{\theta}^2 + \frac{1}{2}m\dot{y}_2^2 \tag{3.1}$$

while the total potential energy U can be obtained as

$$U = -mgy = -mg(y_1 + y_2) \tag{3.2}$$

where θ and y_1 denote, respectively, the angular and vertical displacements of the object COM, respectively, caused by the rotational slip, while y_2 is the vertical displacement caused by the translational slip. Here, m and I denote the mass and moment of inertia of the object about the axis of rotation[1]. From Figure 3.1, it is clear to see that $y_1 = r\sin(\theta)$ where r is the distance of the center of the mass from the rotation axis. Now, the Lagrangian function can be written as :

$$\begin{aligned} L \quad &= T - U \\ &= \tfrac{1}{2}I\dot{\theta}^2 + \tfrac{1}{2}m\dot{y}_2^2 + mg(r\sin(\theta) + y_2) \end{aligned} \tag{3.3}$$

By using the Euler-Lagrange equations [41] ,we can obtain the system dynamics as follows

$$m\dot{v} = mg - \mu F_a \tag{3.4}$$

$$I\dot{\omega} = mgr\cos(\theta) - \beta F_a \tag{3.5}$$

where v and w denote the translational and rotational slip velocities, respectively. Since it is not possible to directly control and apply the gripper force $F_a(t)$, we model the incremental displacement $x_g(t)$ of the gripper as proportional to the applied force such that

$$F_a \propto x_g \tag{3.6}$$

---

[1]Technically, for an arbitrary object, the moment of inertia I in this formulation is a function of both y_2 and θ but for simplicity of modeling, I is assumed to be fixed assuming limited object slipping before control effectively immobilizes it in the application scenario considered here.

the time derivative of which can be related to the control input signal, the gripper velocity $v_g(t)$, as follows

$$\dot{F}_a = \kappa v_g. \tag{3.7}$$
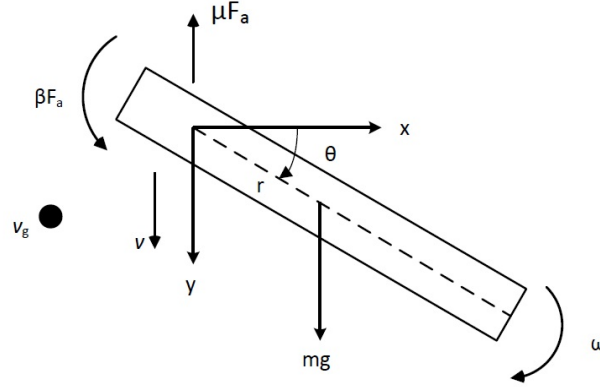
Figure 3.1: Free Body Diagram of a Rotating and Slipping Object within the Fingers of a Robotic Gripper

Assumption: While all objects are deformable to one extent or another (and deformation will be seen during subsequent experiments), this paper primarily deals with objects with medium-to-high stiffness objects which for purposes of control design will devolve to a rigidity assumption.

Control Design and Stability Analysis

Given (3.4), (3.5), and (3.7) as the overall system dynamics model, we design a switched adaptive controller design that is shown to immobilize translational and rotational slippage of the target object constrained within the fingers of a robotic gripper. In order to simplify the analysis, we assume a timescale separation where the desired force is generated in a slow outer loop which then acts as the setpoint for a fast inner loop to command the gripper velocity to converge the desired

23

force to the actual force using a simple proportional controller. For the outer loop, we switch (state-based switching) appropriately between desired forces adaptively generated by the linear-motion based dynamics and the angular-motion based dynamics. A stability analysis is presented for the switched system using a common Lyapunov function which shows that the linear velocity v and angular velocity ω converge to the origin asymptotically. In the next three subsections, F_a is considered to be the control input into the system based on our scale separation assumption stated earlier.

Linear Motion Based System

By defining $a = m/\mu$, we rewrite the dynamics of (3.4) as follows

$$a\dot{v} = ag - F_a \tag{3.8}$$

from which we can design a control input F_a^v based solely on the linear-motion based as follows

$$F_a^v = \hat{a}g + k_1 v. \tag{3.9}$$

where $k_1 > 0$ is a control gain and $\hat{a}(t)$ is a yet to be designed adaptive parameter estimate. Given a Lyapunov function $V_1(t)$ defined as follows

$$V_1 = \frac{1}{2}av^2 + \frac{1}{2}\gamma_1^{-1}\tilde{a}^2 \tag{3.10}$$

where $\tilde{a} \triangleq a - \hat{a}$ is a parameter estimation error and $\gamma_1 > 0$ is a control input, a gradient type adaptive update law of the form

$$\dot{\hat{a}} = \gamma_1 gv \tag{3.11}$$

24

yields a time derivative of $V_1(t)$ along the trajectories of (3.8), (3.9), and (3.11) as follows

$$
\begin{aligned}
\dot{V}_1 &= \tilde{a}gv - k_1v^2 + \gamma_1^{-1}\tilde{a}(-\gamma_1 gv) \\
&= -k_1v^2 < 0
\end{aligned}
\tag{3.12}
$$

From (3.10) and (3.12), it can be shown that $v(t) \in \mathcal{L}_2 \cap \mathcal{L}_\infty$ while $\tilde{a}(t) \in \mathcal{L}_\infty$. Given the closed-loop velocity dynamics

$$
a\dot{v} = \tilde{a}g - k_1v
$$

it is clear to see that $\dot{v}(t) \in \mathcal{L}_\infty$. Now, using Barbalat's Lemma [37][38], it can be proved that $\lim_{t\to\infty} v(t) = 0$. It follows also from the above equation that $\lim_{t\to\infty} \tilde{a}(t) = 0$ for the linear system standing in isolation.

Angular Motion Based System

By defining $b = mgr/\beta$, we rewrite the dynamics of (3.5) as follows

$$
\frac{I\dot{\omega}}{\beta} = b\cos\theta - F_a
\tag{3.13}
$$

from which we can design a control input F_a^ω based solely on the angular-motion based as follows

$$
F_a^\omega = \hat{b}\cos\theta + k_2\omega.
\tag{3.14}
$$

where $k_2 > 0$ is a control gain and $\hat{b}(t)$ is a yet to be designed adaptive parameter estimate. Given a Lyapunov function $V_2(t)$ defined as follows

$$
V_2 = \frac{I\omega^2}{2\beta} + \frac{1}{2}\gamma_2^{-1}\tilde{b}^2
\tag{3.15}
$$

where $\tilde{b} \triangleq b - \hat{b}$ is a parameter estimation error and $\gamma_2 > 0$ is a control input, a gradient type adaptive update law of the form

$$\dot{\hat{b}} = \gamma_2 \omega \cos \theta \tag{3.16}$$

yields a time derivative of $V_2(t)$ along the trajectories of (3.13), (3.14), and (3.16) as follows

$$\begin{aligned} \dot{V}_2 &= \tilde{b} \cos \theta \omega - k_2 \omega^2 + \gamma_2^{-1} \tilde{b} \left(-\gamma_2 \omega \cos \theta \right) \\ &= -k_2 \omega^2 < 0 \end{aligned} \tag{3.17}$$

From (3.10) and (3.12), it can be shown that $\omega(t) \in \mathcal{L}_2 \cap \mathcal{L}_\infty$ while $\tilde{b}(t) \in \mathcal{L}_\infty$. Given the closed-loop velocity dynamics

$$\frac{I\dot{\omega}}{\beta} = \tilde{b} \cos \theta - k_2 \omega$$

it is clear to see that $\dot{\omega}(t) \in \mathcal{L}_\infty$. Now, using Barbalat's Lemma [37][38], it can be proved that $\lim_{t \to \infty} \omega(t) = 0$. It follows also from the above equation that $\lim_{t \to \infty} \tilde{b}(t) = 0$ for the rotational system standing in isolation as long as $\theta \in (-\pi/2, \pi/2)$.

Switched Adaptive System

In order to reconcile the disparate designs of the gripper force F_a as given by (3.9) and (3.14) above, we propose the unified switching control law

$$F_a = \max\left(F_a^v, F_a^\omega \right) \tag{3.18}$$

which is motivated intuitively by the fact that the larger of the two forces would be enough to immobilize both translational and rotational motions. To rigorously prove stability, we can now consider the two cases, namely $F_a^v > F_a^w$ and $F_a^v < F_a^w$ by utilizing the following common Lya-

punov function

$$
\begin{aligned}
V_3 &= V_1 + V_2 \\
&= \frac{1}{2}av^2 + \frac{1}{2}\gamma_1^{-1}\tilde{a}^2 + \frac{I\omega^2}{2\beta} + \frac{1}{2}\gamma_2^{-1}\tilde{b}^2
\end{aligned}
\tag{3.19}
$$

Case 1 ($F_a^v > F_a^w$): In this case, the system evolves along the following closed-loop dynamics

$$
\begin{aligned}
a\dot{v} &= \tilde{a}g - k_1 v \\
\dot{\hat{a}} &= -\gamma_1 gv \\
\frac{I\dot{\omega}}{\beta} &= b\cos\theta - \hat{a}g - k_1 v \\
\dot{\hat{b}} &= -\gamma_2 \omega \cos\theta
\end{aligned}
\tag{3.20}
$$

The derivative of $V_3(t)$ along the dynamics of (3.20) yields

$$
\dot{V}_3 = -k_1 v^2 + \hat{b}\omega\cos\theta - F_a^v\omega.
\tag{3.21}
$$

After adding and subtracting the term $k_2\omega^2$ on the right hand side of (3.21) and rearranging the terms, we can rewrite $\dot{V}_3(t)$ as follows

$$
\begin{aligned}
\dot{V}_3 &= -k_1 v^2 - k_2\omega^2 - F_a^v\omega + \left(\hat{b}\cos\theta + k_2\omega\right)\omega \\
&= -k_1 v^2 - k_2\omega^2 - (F_a^v - F_a^w)\omega
\end{aligned}
\tag{3.22}
$$

Sine the physical constraints of the problem restrict $\omega(t) \geq 0^2$, the last term on the right hand side of the above expression is always negative as long as $F_a^v > F_a^w$. Thus, it is clear to see that $\dot{V}_3(t)$ can be upperbounded as follows

$$
\dot{V}_3 \leq -k_1 v^2 - k_2\omega^2 < 0.
\tag{3.23}
$$

---

[2]By examining the system dynamics, it can be seen that the system is indeed symmetric with respect to clockwise or anticlockwise rotation. The practical import of this is that if the system ends up at the other extreme during a pendulum motion (at which point $\omega = 0$), the angular velocity can be reset to be positive in the other direction which effectively leaves the model and, hence, the controller unchanged.

Case 2 ($F_a^v < F_a^w$)**:** In this case, the system evolves along the following closed-loop dynamics

$$a\dot{v} = ag - \hat{b}cos(\theta) - k_2\omega$$
$$\dot{\tilde{a}} = -\gamma_1 gv$$
$$\frac{I\dot{\omega}}{\beta} = \tilde{b}\cos\theta - k_2\omega \qquad (3.24)$$
$$\dot{\tilde{b}} = -\gamma_2\omega\cos\theta$$

The derivative of $V_3(t)$ along the dynamics of (3.24) yields

$$\dot{V}_3 = -k_2\omega^2 + \hat{a}gv - F_a^\omega v. \qquad (3.25)$$

After adding and subtracting the term k_1v^2 on the right hand side of (3.21) and rearranging the terms, we can rewrite $\dot{V}_3(t)$ as follows

$$\dot{V}_3 = -k_1v^2 - k_2\omega^2 - F_a^\omega v + (\hat{a}g + k_1v)v$$
$$= -k_1v^2 - k_2\omega^2 - (F_a^\omega - F_a^v)v \qquad (3.26)$$

Sine the physical constraints of the problem ensure that $v(t) \geq 0$, the last term on the right hand side of the above expression is always negative as long as $F_a^\omega > F_a^v$. Thus, it is clear to see that $\dot{V}_3(t)$ can be upperbounded in the same manner as indicated in (3.23).

From (3.19) and (3.23), it can be shown that $v(t), \omega(t) \in \mathcal{L}_2 \cap \mathcal{L}_\infty$ while $\tilde{a}(t), \tilde{b}(t) \in \mathcal{L}_\infty$ regardless of how the system switches between Case 1 and Case 2. Furthermore, from (3.20) and (3.24), it can be seen that $\dot{v}(t), \dot{\omega}(t) \in \mathcal{L}_\infty$. Now, using Barbalat's Lemma [37][38], it can be proved that $\lim_{t\to\infty} v(t), \omega(t) = 0$ for the switched adaptive system representing the outer loop. The

28

overall inner and outer-loop switched adaptive control system design can be written as follows

$$F_d^v = \hat{a}g + k_1 v$$
$$\dot{\hat{a}} \triangleq \gamma_1 gv$$
$$F_d^\omega = \hat{b}cos(\theta) + k_2\omega$$
$$\dot{\hat{b}} \triangleq \gamma_2\omega cos(\theta)$$
$$F_d = \max(F_d^v, F_d^\omega)$$
$$v_g = -k_3\left(F_a - F_d\right)$$

(3.27)

where $k_3 > 0$ is a control gain. As can be seen in the block diagram shown in Figure 3.2, the slow outer loop stipulates the desired gripper force F_d using the switching adaptive controller that selects the maximum between $F_d^v(t)$ and $F_d^\omega(t)$. Furthermore, the fast inner loop converges $F_a(t)$ to $F_d(t)$ by applying the appropriate gripper velocity command v_g to achieve force tracking with zero steady-sta
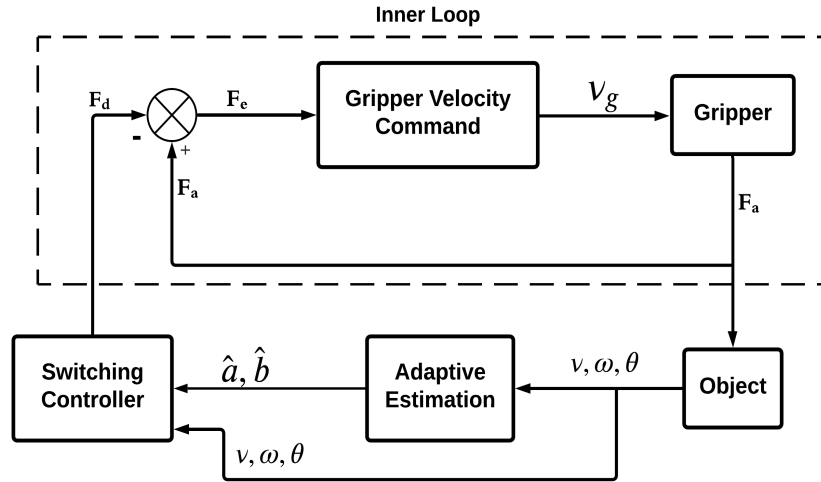
Figure 3.2: Block diagram of adaptive grasping controller powered by a switched system for assigning the desired grippping force

The Sensorized Gripper Prototype

To implement the proposed adaptive algorithm for slippage prevention, the two-finger gripper of UCF-MANUS assistive robot [36] was modified by attaching 3-D printed frames as shown in Figure 3.3. Acrylonitrile Butadiene Styrene (ABS) plastic material was used for fabricating these frames which were designed with cavities and channels with appropriate sizes to allow for embedding the force and slip sensors needed for this research. While one force sensor has been mounted in the left gripper finger frame, two laser-based slip sensors have been mounted $35mm$ apart in the cavity of the right finger one as shown in Figure 3.3(a). The details of our sensor configuration are described below.

Force Sensor

For measuring force, a FlexiForce A201 Force Sensing Resistor (FSR) with range of $0N - 111N$ [42] was fixed between two metal plates of a hinge for freely conveying applied force and then mounted on the gripper finger frame as shown in Figure 3.3(a) and 3.3(d). The FSR was covered with a small plastic disc to direct the force from upper plate to the active sensing area (which is a 0.375" diameter circle) and also to mitigate the nonlinear behavior of the FSR. A small round anti-slip pad was mounted on the outer plate of the hinge as well as on the opposite finger frame providing known contact areas. To calibrate the FSR, a set of known weights ($0 - 1000g$) was applied to measure the corresponding voltages followed by curve fitting. For interfacing purpose, Phidget Interface Kit 8/8/8 I/O Board featured with high-bandwidth data acquisition was utilized with a FlexiForce Adapter to read force data from the FSR with a sampling rate of 62.5Hz.
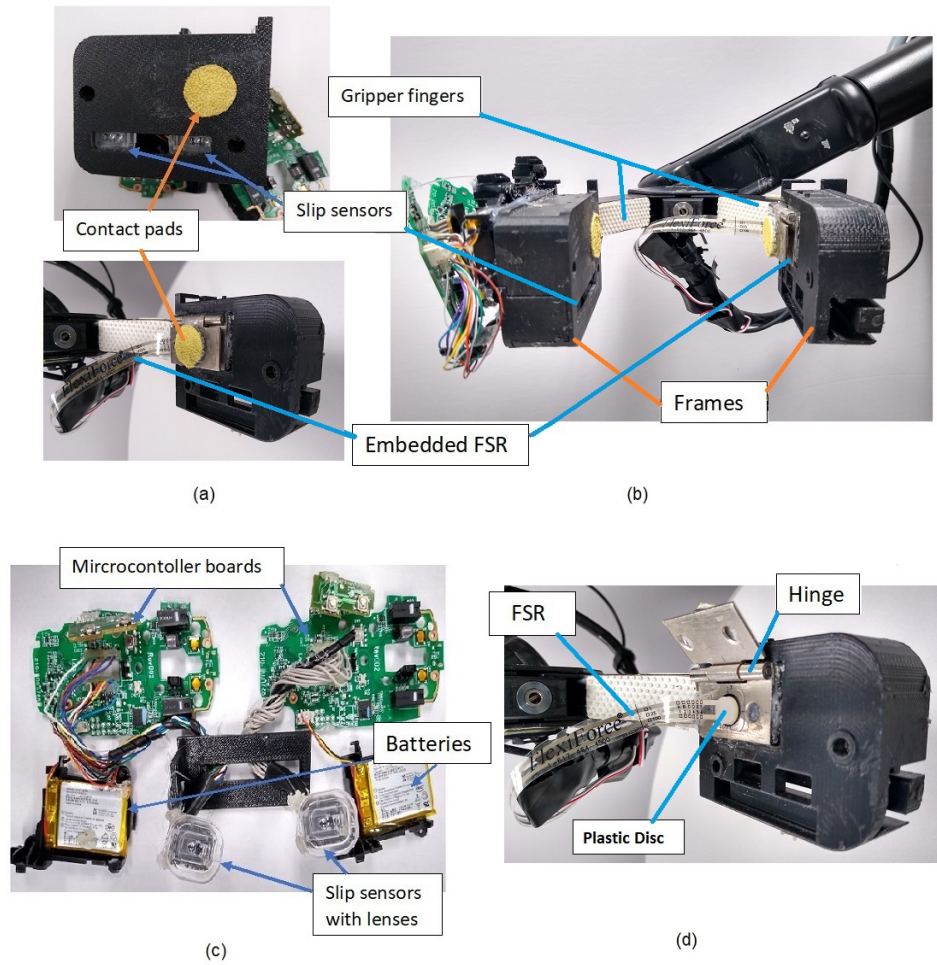
Figure 3.3: (a) Frames with sensors (b) sensorized gripper (c) Laser slip sensors with their micro-contoller boards and batteries (d) FSR sensor mounted on the gripper frame.

Slip Sensors

We decided to use a non-contact type of slip sensor, specifically the darkfield high-precision laser sensor, for slip detection of grasped objects. The darkfield sensor and its microcontroller interface board were extracted from a Logitech MX Anywhere 2S Mouse device and the two darkfield sensors were reconnected to their respective interface board with longer extension wires as shown

in Fig.3.3(c). These sensors create a micro-road map of the surface and detect position changes that allows them to track those changes accurately on virtually any surface including very glossy and transparent objects [40]. The laser sensor is supported by a polycarbonate round lens for directing illumination and optical imaging necessary for proper operation of the sensor. The board interface has a rechargeable 500 [mAh] battery and can connect to the computer port wirelessly.

The laser sensors can be programmed to have a maximum resolution of 4000 [DPI] (or 6.35×10^{-3} [mm/pixel]) with a 1000 [Hz] polling rate which is sufficient for our slippage detection algorithm. As the control algorithm was run in a Microsoft WINDOWS environment, WM_INPUT message was utilized along with the GetRawInputData function to retrieve raw data from the human inter-facing device (HID) stack which in our case are the two laser sensors. WM_INPUT message can distinguish between similar type of devices, *e.g.,* mouse-like devices, connected to the computer which allowed us to use two laser sensors running simultaneously. After position data from both slip sensors was received, it was processed to obtain the respective slipping velocities as follows. First, an exponential smoothing function was utilized to smooth the position data. Then, a time derivative of the smoothed output was filtered using a third order low-pass Butterworth filter with a 45 [Hz] cutoff frequency to obtain slipping velocity signal with low noise [19]. The two laser mouse sensors were used to measure the linear y-direction slip velocities v_1 and v_2 of the grasped object from which the common mode (translational) and differential mode (angular) slip velocities of the object were estimated as

$$v = \frac{v_1 + v_2}{2} \tag{3.28}$$

and

$$\omega = \frac{v_2 - v_1}{d} \tag{3.29}$$

where d is the distance between the two laser sensors which is 35 [mm] for our prototype.

Implementation

Experimental Setup and Procedure

The UCF-MANUS platform [36] together with our new sensorized robotic gripper was used as the experimental environment. For testing the implementation of our proposed algorithm, we picked a variety of objects within the lifting range of the UCF-MANUS gripper. The comprehensive experimental studies examined different weights, textures, geometries, and orientations of objects with respect to the contact point by the gripper fingers. This allowed us to verify the robust performance of the algorithm in meeting the goals extensively discussed in the introduction and problem statement section of the paper. As shown in Figure 3.4, the objects included cereal boxes with different weights (68 [g], 113 [g], and 380 [g]) as well as three plastic bottles of weights (113 [g] , 275 [g], and 284[g]) with different contents (water and sand) to capture the effect of change in moment of inertia of objects during slippage. The minimal (ground truth) grasping force, F_{gt}, for each object was found by repeatedly setting an increasing amount of desired force F_d manually in the controller and applying gripper velocity $v_g = -k_3 \left(F_a - F_d \right)$ to convergence until reaching the minimum force F_d that immobilized an object in its particular configuration. Having found F_{gt} in this manner, it can be compared with the automated final applied grasping force for each object obtained via application of the proposed closed-loop adaptive algorithm as implemented through (3.27). We also observed the degree of deformation of the objects after the algorithm had been executed successfully. The controller gains and adaptive estimation parameter initial conditions used for all experiments are shown as follows

$$k_1 = 400, k_2 = 20, k_3 = 0.95$$
$$\gamma_1 = 35, \gamma_2 = 16 \tag{3.30}$$
$$\hat{a}\left(0 \right) = 2.5/g, \hat{b}(0) = 2.5$$

To test the proposed closed-loop adaptive algorithm, a two-step grasping process was implemented consisting of *initial grasping* and *adaptive regrasping* as described below.

Figure 3.4: Objects grasped using the proposed algorithm. From left to right: Box 1: 340 [g] filled with sand, Box 2: 68 [g], Box 3: 113 [g], Sand Bottle: 113 and 284 [g], Water Bottle: 113 [g], and Water Bottle(cylindrical): 275 [g].

Initial Grasping

The target object initially is static and resting on a base. Since our sensorized two-finger gripper exhibits asymmetry in the type of sensors used (*i.e.,* a force sensor on the left finger and slip sensors on the right finger), we require valid measurements from both the slip and force sensors to establish initial object contact with both fingers. We determined experimentally that an initial force measurement of greater than 1.5 [N] coupled with a detected slip velocity magnitude of at least 0.1 [mm·s^{-1}] satisfies the initial contact condition. Meeting these contact conditions concludes the initial grasping phase with the gripper exerting a minimal grasping force on the object. At the end of this phase, the resting base of the object is removed so it is only under gravity and gripper forces.

Adaptive Regrasping

If translational and/or rotational slippage is detected upon removing the object base (i.e., the initial grasping force was less than the minimal forced needed for immobilization), the proposed closed-loop adaptive regrasping as described by (3.27) is carried out until slippage ceases (i.e., $v, \omega \to 0$) and the force error ($F_e \triangleq F_a - F_d$) converges to near zero. At the conclusion of this phase, we measure the force deviation $F_{dev} \triangleq F_a - F_{gt}$ as the difference between the final gripper applied force F_a and the requisite minimal ground truth force F_{gt} as computed earlier with the open-loop process described above. We also observe the corresponding degree of deformation of the object.

Experimental Results

Overall, six experiments were conducted. In the first two experiments, Box 1 (340 [g]) and the Sand Bottle (284 [g]) were placed with their center of gravity (CG) within the gripper fingers such that the resulting motion was predominantly translational. In the remaining four experiments, the objects were placed with their CG outside the extent of the fingers such that the slipping motion was mainly rotational. During all experiments, the amount of force applied during the *initial grasping* phase was lower than minimal such that rotational/ translational slip was observed between the gripper fingers and the objects during the *adaptive regrasping* phase.

Before and after pictures with predominantly translational slipping seen in the first two experiments are shown in Figure 3.5. The force and motion data from these experiments plotted in Figures 3.6 and 3.7 show that closed-loop adaptive regrasping was activated successfully to ensure convergence of the translational slip velocity to zero within 2.5 [s] following initiation of slipping. As expected, the objects show no rotational slippage during the course of these two experiments. Similarly, the error between the desired and actual forces converged to near zero as well. Table 3.1 shows that the

35

force deviation F_{dev} was 5.49% and 3.8%, for the box and the water bottle, respectively. This small

force deviation is reflected in the lack of object deformation observed during both experiments.
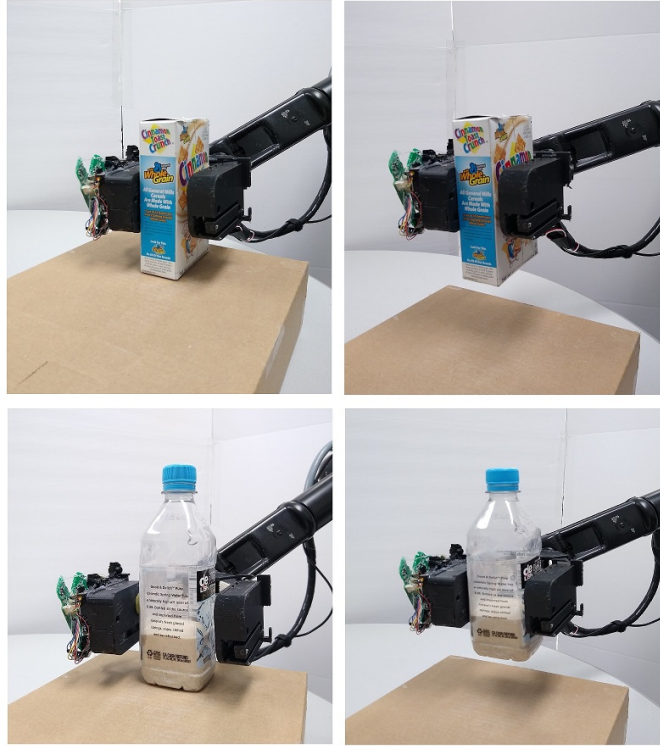
Figure 3.5: A side-by-side view of the grasped objects before and after closed-loop adaptive re-grasping algorithm has been executed for translational slippage.

Before and after pictures with predominantly rotational slipping along with some translational

slipping from the next four experiments are shown in Figure 3.8. Force and motion data from these

experiments can be seen in Figures 3.9-3.12 from which it is clearly seen that closed-loop adaptive

regrasping was activated successfully to ensure convergence of the rotational and translational slip

velocities to zero within 3.5 [s] following initiation of slipping. Due to the object configuration,

data clearly shows that the rotational velocity was the dominant part of the motion even as the

translational velocity was clearly present. Data also shows the close convergence of the actual

applied actuator force F_a to the maximum of the desired rotational (F_d^ω) and translation (F_d^v)

Figure 3.6: Slip detection and Adaptive re-grasping of a 340 [g] box containing sand. Initial grasping stage lasts between t = 0 [s] and t = 3.48 [s] using an initial grasp force of 1.7 [N]. Robot starts lifting the bottle at t = 3.48 [s] and the algorithm detects translational slipping at which time the proposed closed-loop adaptive algorithm executes to stop slipping using final grasping force of 5.38 [N].

forces. Table 3.2 shows that the force deviation F_{dev} was between 2.78% (for Box 3) and 7.75% (for Water bottle). Low to no deformation was observed for all objects tested.

Further Experimental Results

Two more experiments were conducted to show that the proposed algorithm was able successfully to prevent slippage (a) for an object with a non-flat surface (cylindrical in this case), and (b) with a different gripper orientation (rolled in this case). A cylindrical water bottle (275 [g]) was tested for predominantly translational slipping as shown in Figure 3.13 (top). The force and motion data from this experiment plotted in Figure 3.14 show that the closed-loop adaptive regrasping was activated successfully to ensure convergence of the translational slip velocity to zero within 1.7 [s]

Figure 3.7: Slip detection and Adaptive re-grasping of a 284 [g] bottle containing sand. Initial grasping stage lasts between t = 0 [s] and t = 3.28 [s] using an initial grasp force of 1.7 [N]. Robot starts lifting the bottle at t = 3.28 [s] and the algorithm detects translational slipping at which time the proposed closed-loop adaptive algorithm executes to stop slipping using final grasping force of 4.36 [N].

following initiation of slipping with zero error between the desired and actual forces. Table 3.3 shows that the force deviation F_{dev} was 6.1% for cylindrical water bottle resulting in no observed object deformation during the experiment. In Figure 3.13 (bottom), the Box 3 (113 [g]) was tilted with respect to the gravity axis so that the gripper would need to grasp it with a 30 [degree] roll angle (ϕ). In this case, the acceleration of gravity (g) component in the direction of the gripper plane (i.e. $g\cos(\phi)$) was considered in the control algorithm equations of (3.27). This is easily implementable since the complete 3-DOF attitude of the robot gripper is available in real-time from the robot kinematics[3]. The experimental results for this case seen in Figure 3.15 show clearly that rotational velocity was the dominant motion along with some amount of translational velocity.

---

[3]We note here that another simplification would be to consider $g\cos\phi$ to be an unknown parameter and subsume it into the parameter adaptation for a resulting in an even simpler formulation for the implementation given in (3.27).

Table 3.1: Desired Force, Applied Force, Ground Truth Grasping Force, and Deformation Degree Data for Translational slipping case

	Box 1(340 [g])	Sand Btl.(284 [g])
F_d	5.55	4.59
F_a	5.38	4.36
F_{gt}	5.10	4.20
F_{dev}	0.28	0.16
$\%F_{dev}$	5.49	3.80
Deformation	none	none

Table 3.2: Desired Force, Applied Force, Ground Truth Grasping Force, and Deformation Degree Data for Rotational slipping case

	Box 2	Box 3	Sand Btl.	Water Btl.
F_d	4.05	5.98	6.79	8.49
F_a	3.54	5.55	7.03	8.62
F_{gt}	3.30	5.40	6.80	8.00
F_{dev}	0.24	0.15	0.23	0.62
$\%F_{dev}$	7.27	2.78	3.38	7.75
Deformation	none	low	none	low

It can be clearly seen that the closed-loop adaptive regrasping was activated successfully to ensure convergence of the translational slip velocity to zero within 2 [s] following initiation of slipping. Furthermore, data shows that the actual applied actuator force F_a converged to the maximum of the desired rotational force (F_d^ω). Table 3.3 shows that the force deviation F_{dev} was 3.5% with no visual deformation of the object.

Practical Application

For practical applications such as object retrieval (or pick-and-place), the algorithm is embedded in an overall grasping scheme as shown in Figure 3.16 which includes upper bounds on time and

39

Figure 3.8: A side-by-side view of the grasped objects before and after closed-loop adaptive re-grasping algorithm has been executed for predominantly rotational slippage.

maximum amount of slip allowed. For example, to allow for user intervention, we set a time-out condition of 10 [s] for completion of the gripping process. If the object continues to slip beyond a limit, we continue to regress to a series of other suboptimal regrasping schemes including open-loop adaptive regrasping (where the gripper is allowed to close till it detects force flatness [18]) and hardware-limited (available by default in the gripper) regrasping if further slip is detected. Online
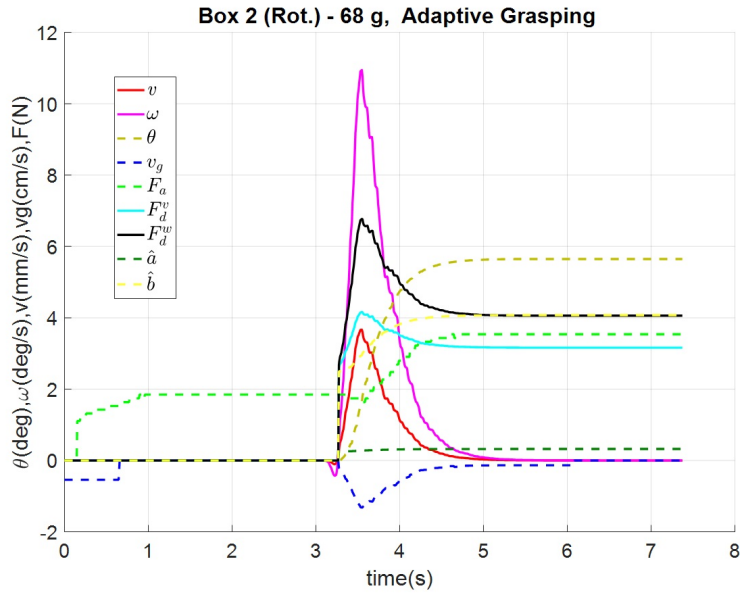
Figure 3.9: Slip detection and Adaptive re-grasping of 68 [g] box. Initial grasping stage lasts between t = 0 [s] and t = 3.26 [s] using an initial grasp force of 1.85 [N]. Robot starts lifting the bottle at t = 3.26 [s] and the algorithm detects rotational slipping at which time the proposed closed-loop adaptive algorithm executes to stop slipping using final grasping force of 3.54 [N].

video demonstrations [43] performed in the Assistive Robotics Laboratory with the UCF-MANUS

are available which show the application of the proposed adaptive algorithm. The Table 3.4 shows

a comparison of our algorithm illustrated in this chapter with state-of-the-art work in [7].
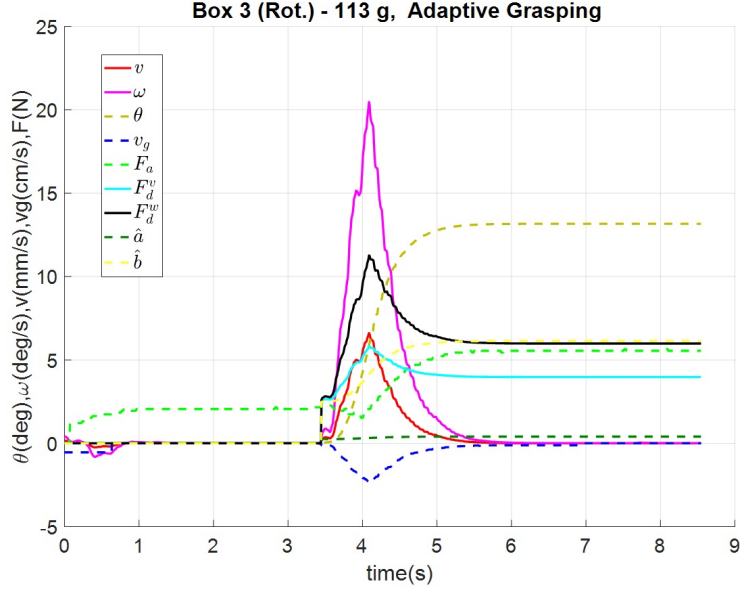
Figure 3.10: Slip detection and Adaptive re-grasping of 113 [g] box. Initial grasping stage lasts between t = 0s and t = 3.44s using an initial grasp force of 2N. Robot starts lifting the bottle at t = 3.44s and the algorithm detects rotational slipping at which time the proposed closed-loop adaptive algorithm executes to stop slipping using final grasping force of 5.55 N.

Table 3.3: Desired Force, Applied Force, Ground Truth Grasping Force, and Deformation Degree Data for Transaltional slipping (cylindrical object) case, and Rotational slipping with Rolling Gripper case

	Water Btl.(cyl)	Box 3
F_d	4.36	4.57
F_a	4.35	4.14
F_{gt}	4.10	4.0
F_{dev}	0.25	0.14
$\%F_{dev}$	6.1	3.5
Deformation	none	none
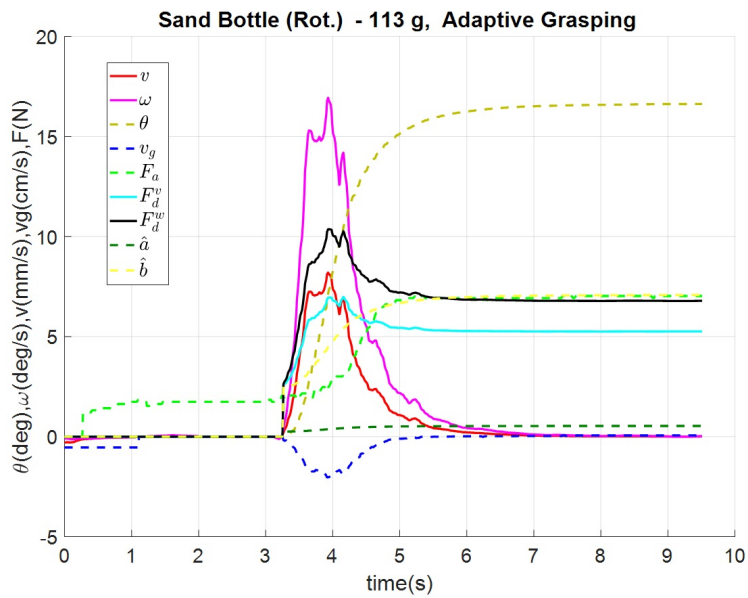
Figure 3.11: Slip detection and Adaptive re-grasping of a 113 [g] bottle containing sand. Initial grasping stage lasts between t = 0 [s] and t = 3.24 [s] using an initial grasp force of 1.8 [N]. Robot starts lifting the bottle at t = 3.24 [s] and the algorithm detects rotational slipping at which time the proposed closed-loop adaptive algorithm executes to stop slipping using final grasping force of 7.03 [N].
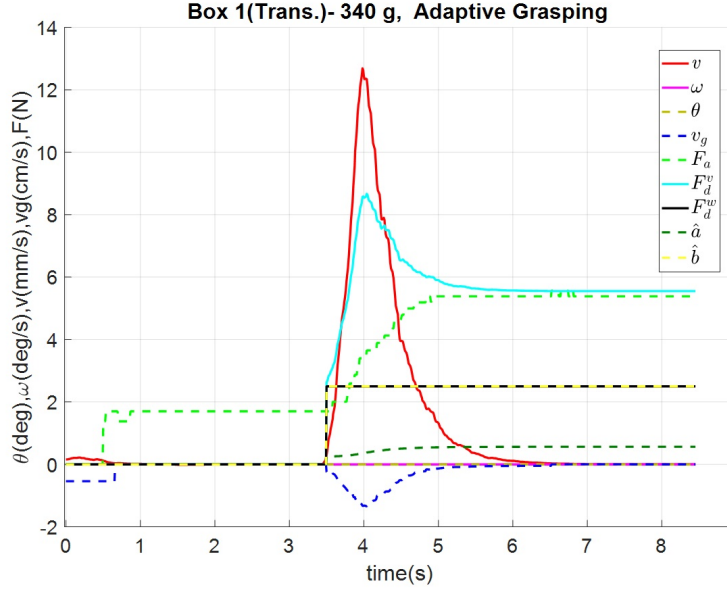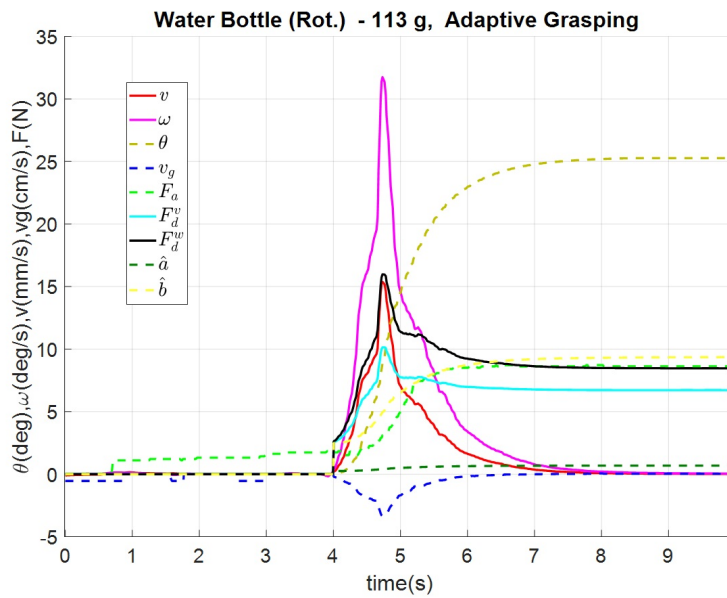
Figure 3.12: Slip detection and Adaptive re-grasping of a 113 [g] bottle containing water. Initial grasping stage lasts between t = 0 [s] and t = 4 [s] using an initial grasp force of 1.84 [N]. Robot starts lifting the bottle at t = 4 [s] and the algorithm detects rotational slipping at which time the proposed closed-loop adaptive algorithm executes to stop slipping using final grasping force of 8.62 [N].
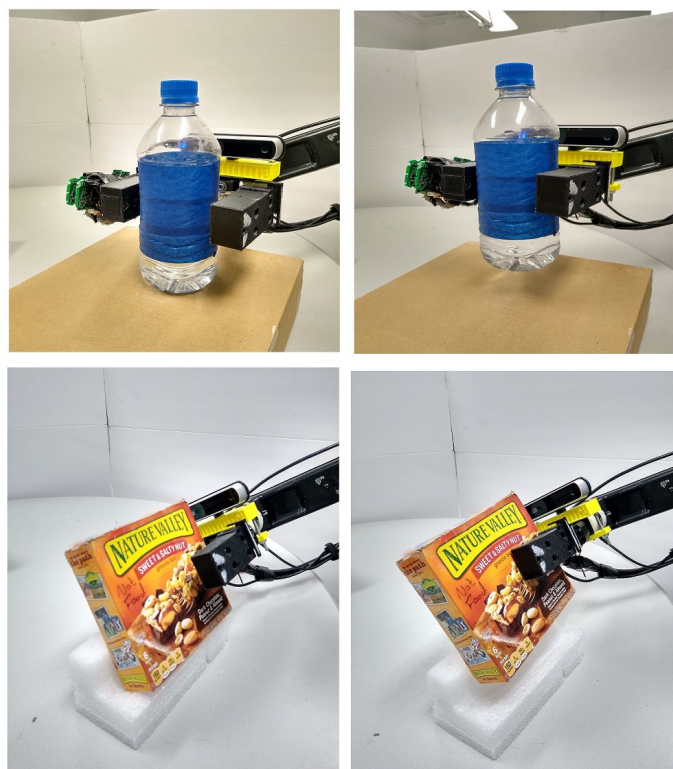
Figure 3.13: A side-by-side view of the grasped objects before and after closed-loop adaptive re-grasping algorithm has been executed for translational slippage with cylindrical object (top), and rotational slippage with rolling gripper of 30° (bottom).
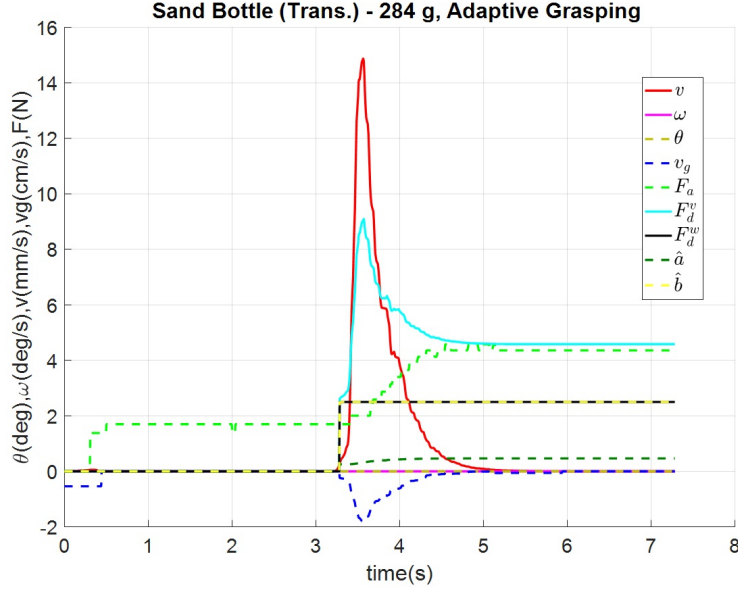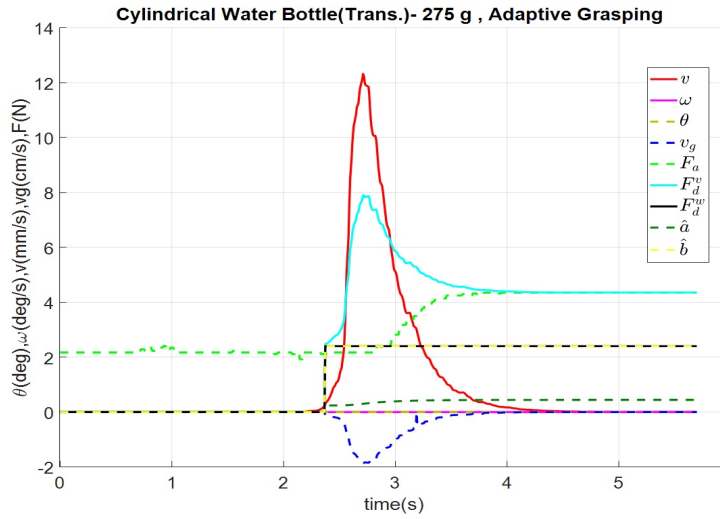
Figure 3.14: Slip detection and Adaptive re-grasping of a 275 [g] cylindrical bottle containing water. Initial grasping stage lasts between t = 0 [s] and t = 2.4 [s] using an initial grasp force of 2.17 [N]. Robot starts lifting the bottle at t = 2.4 [s] and the algorithm detects translational slipping at which time the proposed closed-loop adaptive algorithm executes to stop slipping using final grasping force of 4.35 [N].

Table 3.4: Comparison of the Algorithm with State-of-the-Art

	Engeberg *et al.*'s work[7]	Our proposed work
Controller approach	Adaptive sliding mode	Switched adaptive controller
Measurement sensors	Strain gauges: normal Force and shear force	FSR:force, Two Laser slip sensors
Slip detection	Indirectly from high frequency vibration of shear force	Directly from slip sensor (slipping velocities)
Stability	asymptotically stable	asymptotically stable / Lyapunov based analysis
Slippage prevention type	Translational only	translational and rotational
Settling time	Not reported	2.5 - 3.5 sec
Object type	Instrumental object (manipulandum) with adjustable stiffness and disturbance weights	real objects with various shapes and weights
Deformation	Low (2.5-5mm)	None – low (0-5mm)
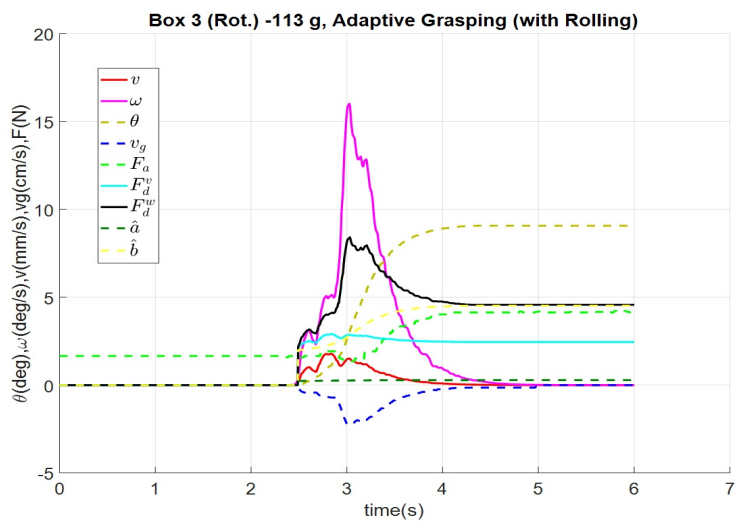
Figure 3.15: Slip detection and Adaptive re-grasping of 113 [g] box with rolling gripper 30°. Initial grasping stage lasts between t = 0s and t = 2.5 [s] using an initial grasp force of 1.6 [N]. Robot starts lifting the bottle at t = 2.5 [s] and the algorithm detects rotational slipping at which time the proposed closed-loop adaptive algorithm executes to stop slipping using final grasping force of 4.14 [N].
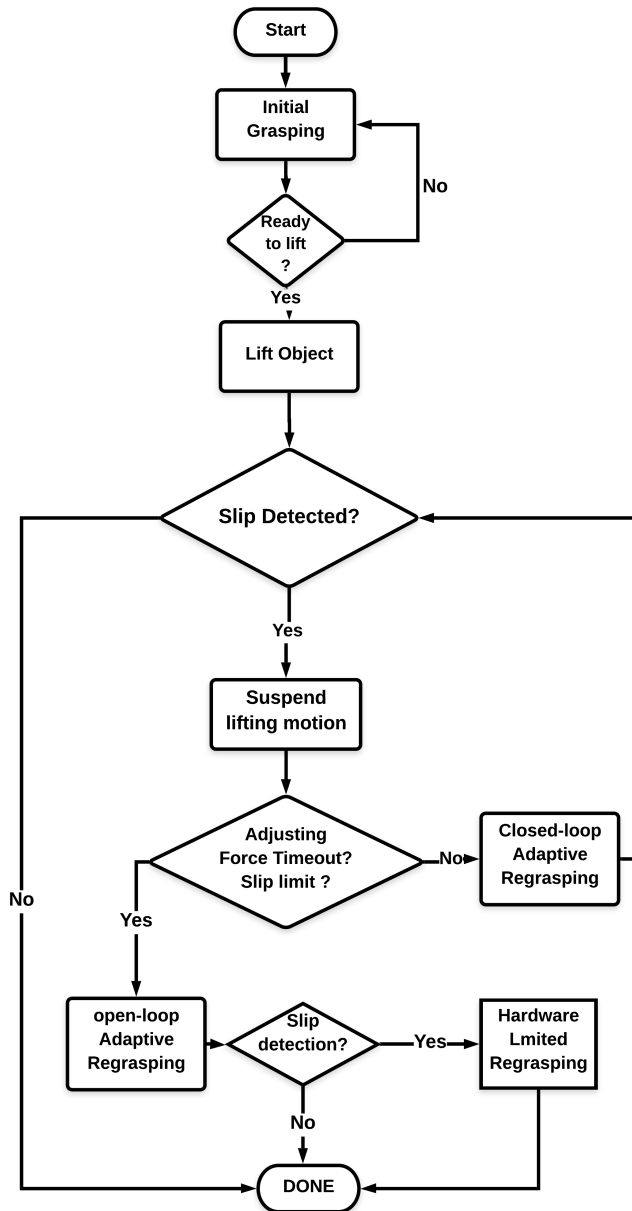
Figure 3.16: Flowchart of the proposed adaptive grasping algorithm

CHAPTER 4: A PUTATIVE MODEL FOR JOINT PROBABILITY DISTRIBUTION OF HUMAN FACTORS RELATED TO HUMAN-ROBOT INTERACTION (HRI)

Experimental Methodology

Here we utilized data generated by the experiments conducted by Paperno *et al.* [29] to analyze the human factors and find a model for the joint probability distribution of them.

Participants

In this research study, 93 able-bodied individuals (46 Male and 47 Female) between the ages of 18 and 63 were recruited from UCF and the surrounding metropolitan areas. According to the Internal Review Board (IRB), some population :prisoners, disabled, cognitively impaired, elderly (over 65), or juvenile (under 18) were excluded from participation in this study.

Materials and Apparatus

Robotic Platform Setup

A 6 degrees-of-freedom (6DOF) assistive robotic arm (called UCF-MANUS ARM) developed by Exact Dynamics Inc. was utilized in this study. It can reach an object with a maximum distance of $80cm$ from the center of the base frame and it has ability to lift 4.5 Ibs ($2.041kg$) object as a maximum wight. A comprehensive interface and automated grasping algorithms have been designed

and added to the robotic arm [44]-[46]. A graphical user interface (GUI) comprised of a view from a camera attached to the robot gripper, a feedback panel, and various buttons for manipulating the robot's arm and hand motions allowed participants to control the robot.The software operated on a Windows machine and the GUI was displayed on a 12 x 9 inch color desktop monitor. All of the participants used a mouse to click on desired functions on the screen to control the robotic manipulator manually. To keep the robot moving in the direction indicated by the clicked functional button on the screen, the system needed that the mouse button be held down continuously. The experimental configuration was created to resemble the positioning of a WMRA on the side of a wheelchair for a user. In order to attain this, Near the user, a table and a bookcase were installed. The table was put in front of the robotic arm, while the bookcase was placed next to the table on the participants' right side. The entire setup is depicted in the Figure 4.1

Figure 4.1: Setup of experiment with the UCF-MANUS was located to the right of the user, who controlled it with the mouse and the GUI displayed on the screen.[29]

Measurement of Human Factors

- Reaction Time (RT): It was measured using Simple Reaction Time test [47]. There is just one visual stimuli, and when it appears, an individual needs to respond by pressing a keyboard button. It measures how long it takes to perceive a stimulus, retrieve data from memory, and produce a muscular response. Response times may thus be used to determine the length of time required for basic thinking processes.The age and overall intellect of a person affect their response speed. Many other factors come into play, such as the circumstances in which people accomplish the task (are they fatigued, hungry, etc.). In addition, the speed is determined by how precise a person want to be. If a person does not want to make mistakes, he or she will slow down. This is known as the speed-accuracy trade off [48]-[49]. In our robot task experiments, an individual is involved in controlling the robotic manipulator manually to perform different tasks including Find and Fetch tasks and Pick and Place tasks. The main feedback to the user is the visual signal through direct viewing or through viewing the environment via the robot mounted camera. After perceiving visual stimuli, the user will process them mentally to interpret them, and then respond by moving the mouse to click on a desired command button on the screen and hold it depressed to control the arm and the hand of the robot. Therefore, if one or more of the processes (perception, processing, and response) are delayed, the reaction time will increase, and the user's performance will decline as consequence especially the time-on-task (ToT). The user may respond to a known stimulus that he or she has previously responded to. In this situation, the reaction time will be shorter since there would be less information to analyze.

- Spatial Ability: It consists of two different factors [50]. First is the spatial visualization (SpV) measured by using Paper Folding test [51]. This factor measures the ability to mentally manipulate and transform 2D and 3D image into other arrangements. The second factor is spatial orientation (SpO) measuring the ability to perceive spatial patterns or to maintain orientation with respect

to objects in space. The Cube Comparison test is used to measure spatial orientation [51]. For our robot experiments, individuals need to utilize their spatial orientation abilities to compare the current position and direction of the robot hand with their owns, and then adjust mentally for any differences so they can move the robot toward the desired position. This will help them to plan the trajectory of the robot hand movements as quickly and accurately as possible to reach and grasp the desired object and move it to another position. This factor will be more relevant when users move the robot hand toward them to bring the object (from tabletop; in front of them, and from bookshelf ; on the right side of them) as they will need to rotate their egocentric reference frame with respect to camera frame. Therefore, any lack on this ability will lead the participants to use longest path and cause some confusion in adjusting their orientations which in turn adds more delay and number of moves in completing task. On the other hand, the participants will use their spatial visualization abilities during grasping the desired object as they need to imagine how the orientation of the gripper should be, so they can rotate it to coincide with the object's one. This is also true when they are utilizing the camera view via screen. They need to manipulate 2D images and transform them into 3D space so they can orient the robot hand to grasp the object. It would be expected that individuals with high spatial visualization abilities would do these rotations without difficulties resulting in fast response and less commands. Therefore, the spatial abilities play an important role in successful performance.

- Visual Perception (VP): The Motor-Free Visual Perception Test (MVPT) was used to evaluate participants' visual perception regardless of their motor ability.[52]. Visual perception is a measure of the brain's capability to receive, interpret, and respond on visual inputs. As a result, it is critical for users to be able to identify the names and locations of command buttons in the GUI. It will assist them in distinguishing the targeted object among the other objects and the table/bookshelf that contains those objects. Also, during object grasping, they need to match the width of the object with the distance between the two fingers of the gripper accurately so they can open those fingers

in continuous movement without pausing.

- Working Memory (WM): This factor was measured by using NAB backward digit span test [53]. It assesses how long an individual can retain pieces of information in a short-term memory. Its capacity is limited and it is thought to be roughly 7-9 items at a time [54]. During controlling the robot, Working memory is required to remember which object has to be grasped so they can plan the movement trajectory with minimum distance and to reduce the time to reach the target. It is also needed for remembering the function of each command and its position on the screen so they can select the correct one quickly without keep trying other commands and as a result, the task will take longer to accomplish, and the number of movements will rise.

- Gross and Fine Dexterity: By using Purdue Pegboard Test, the dexterity of an individual was measured [55]. This test measure two abilities: 1) gross dexterity (GD) in moving arms, hands, and fingers 2) fine dexterity (FD) in coordinating small muscles in movements which involving the synchronization of hands and fingers and usually with eyes. As the individuals control the movement of the robot by moving the mouse device and then choosing and pressing a desired command button among others on the GUI , they need to use their fine motor skills to do so more than using gross dexterity. Therefore, the fine dexterity will play an important role in the user performance and if there is any lack in this dexterity, it will increase the Time-on-Task (ToT).

- Visual Acuity: A standard Snellen visual acuity chart was used to measure the clarity or sharpness of vision[56]. It relates to the spatial resolution of the visual processing system. As mentioned before, the visual feedback is the main signal that the individual will use to control the robot, therefore the clarity of this signal is important especially when reaching the object. While grasping the desired object, the details of its edges are needed so the user can avoid hitting the object and close the two fingers of the gripper properly. Thus, the user performance will be influenced if the participant's vision has defected. It may have less effect if the user depends on the screen to view

the object during the reaching and grasping. The strongest vision (SV) was assigned to the eye with higher score and weakest vision (WV) to the eye with worse performance.

- Depth Perception: Randot Stereotest was used to measure individuals' ability to perceive depth perception [57]. It measures their ability to binocularly discern the distance of an object and see things in three dimensions. The depth perception is important for the users to see the relative position of the robot gripper, desired object, and other objects and also to conceive their sizes. Any deficiency in this ability will lead to low performance as the user cannot estimate the distance between the end-effector of the robot and the target.

Measurement of Performance Metrics

Three criteria were used to assess performance: average Time on Task (ToT), Number of Moves (NoM), and Number of Moves per minute (NoM/min). Both ToT and NoM measures have been used in other works [22] [23] [58], whereas NoM/min is a statistic that is meant to be constant across all tasks, independent of their type or length. The time from the participant's start movement to the conclusion of the activity was recorded as ToT, while The number of instructions the user used to accomplish the task was utilized to calculate NoM.The NoM/min is calculated by dividing the number of moves by the time(in minutes) spent on the task.The final value for each metric for a specific user was calculated by averaging the data for that metric across all of the tasks that the user completed.

Procedure

The participants completed an informed consent form as well as a preliminary demographic questionnaire when they arrived at the lab, then followed by an evaluation of all human variables in-

dicated above.To avoid order effects and tiredness, all tests were delivered in a randomized order except for the reaction time test which was always done first to avoid fatigue impacting the results. As mentioned in the experiment setup, the robot was placed on the right side of user's chair. Participants were then seated in a chair in front of the computer that controlled the robotic manipulator. After that, a brief introduction of the robot given to them. The interface was demonstrated by explaining how each of the commands functioned. After the demonstration, the participants were given up to ten minutes to operate the robot as they wished to ensure that they understood how to control it. They got the opportunity to ask any questions they had about the robot and its operation during this time. Before the ten minutes were over, participants might say that they were satisfied with their abilities, and the experiment would proceed to the next step. Only one of the 93 participants took all ten minutes before going on to the next step. A user took 90 minutes approximately to complete the entire experiment.

Simulated ADL Tasks

Participants were given a total of six tasks to complete using the robotic manipulator. Pick-and-place (PNP) and find-and-fetch (FNF) tasks were used to simulate a collection of typical Activities of Daily Living (ADLs) carried out by a robot [59]. PNP activities needed users to pick up an object and place it in a different spot in the workspace, whereas FNF ones required users to pick up an object and bring it to them. Users were instructed to pick up a standardized object (.81 oz (23g) travel-sized cereal box) and place it at predetermined places marked by blue tape. To complete the tasks, each participant was instructed to control the robot manually using the white command buttons in the GUI shown in Figure 4.1. The robot was reset to a predetermined start position for the user at the beginning of each task. The specific six tasks assigned to the participants can be found in the Table 4.1.

Table 4.1: Simulated ADL Tasks

Task#	Descriptions	Type
T1	Retrieve an object from a tabletop and bring it the participant	Find and Fetch
T2	Move object from one side of the table to the other	Pick and Place
T3	Take object and move it from the top of the table to the bottom of the table	Pick and Place
T4	Retrieve an object from the middle shelf on the bookcase and bring it to the participant	Find and Fetch
T5	Take an object from the top of the bookshelf and move it to the middle shelf	Pick and Place
T6	Take an object from the top of the bookshelf and move it to the tabletop	Pick and Place

Data Analysis

Dependency Analyzing of the Human Factors

Pearson Correlation Test

To study the relationship and dependency between the human factors, the covariance matrix was constructed first to determine the direction of the linear relationship between each pair of factors. In the Table 4.2, the off-diagonal elements of the covariance matrix show the covariance coefficients between each two variables. The positive coefficient indicates that both variables are increasing at the same time. The negative one, on the other hand, indicates that both variables move in opposing directions. [60]. As the human factors were measured in different scales, It is difficult to evaluate the strength of the relationship just on the magnitude of the covariance coefficients. A standardized

56

form of the covariance matrix, i.e. the correlation matrix, was used to measure the strength of the dependency between the human factors. The correlation coefficient of two variables was calculated by dividing the covariance of these variables by the product of the their standard deviations. This converts the scale of the covariance values to $[-1, 1]$. The correlation (or what is called Pearson correlation) coefficients are shown in the Table 4.3 . The r is the Pearson correlation coefficient for each pair of the factors. The closer the coefficient is to $+1$ or -1, the stronger the relationship between the two variables. If it is 0 or close to, there is no linear relationship between the two factors. Cohen's standard was used to evaluate the correlation coefficient to determine the strength of the relationship. The absolute values of r between 0.10 and 0.29 represent a small relationship, between 0.30 and 0.49 represent a medium relationship, and a large relationship is explained by 0.50 and above [61].

Interpretation: From the Table 4.3, one can conclude that: the Spatial Orientation (SpO) is highly correlated with each of the Spatial Visualization (SpV) ($r = 0.67$) and Visual Perception (VP) ($r = 0.60$) significantly with p-value < 0.001. Also, it is noticed that SpV is highly correlated with the VP ($r = 0.61$) significantly with p-value < 0.001. For the dexterity, the Gross Dexterity (GD) and Fine Dexterity (FD) are highly correlated ($r = 0.65$) significantly with p-value < 0.001. The Weakest Vision (WV) and Strongest Vision (SV) are highly correlated ($r = 0.67$) significantly with p-value < 0.001. Some of other human factors show moderate correlation as seen in the Reaction Time (RT) with each of SpO ($r = -0.44$) , SpV ($r = -0.46$), VP ($r = -0.39$), WV ($r = -0.41$) significantly (p-value < 0.001) and with the Working Memory (WM) ($r = -0.32$) significantly (p-value< 0.01). Also, SpO is moderately correlated with WM ($r = 0.30$) and FD ($r = 0.32$) significantly (p-value < 0.01) and with Depth Perception (DP) ($r = -0.35$) significantly (p-value< 0.001). It can be seen also that the SpV and WM are correlated with moderate coefficient ($r = 0.35$) significantly (p-value < 0.001). The VP is moderately correlated with each of GD ($r = 0.31$) significantly (p-value < 0.01) and FD ($r = 0.36$) significantly (p-value < 0.001). Lastly, the

Table 4.2: The Covariance Matrix of the Human Factors

HF	RT	SpO	SpV	VP	WM	GD	FD	WV	SV	DP
RT	8660.56	-464.70	-324.30	-775.41	-54.76	-101.02	-184.68	-8.82	-4.41	6.54
SpO	-464.70	130.70	58.63	144.95	6.44	16.35	27.71	0.34	0.04	-1.61
SpV	-324.30	58.63	58.42	98.60	4.97	4.45	15.83	0.09	0.04	-0.50
VP	-775.41	144.95	98.59	451.86	11.46	32.53	58.62	0.61	0.59	-1.69
WM	-54.76	6.44	4.97	11.46	3.43	0.36	3.60	0.004	0.02	-0.06
GD	-101.02	16.35	4.45	32.53	0.36	24.90	24.79	-0.001	-0.01	-0.36
FD	-184.68	27.71	15.83	58.62	3.60	24.79	58.91	0.12	0.14	-0.37
WV	-8.82	0.34	0.09	0.61	0.004	-0.001	0.12	0.05	0.03	-0.026
SV	-4.41	0.04	0.04	0.59	0.02	-0.01	0.14	0.03	0.04	-0.01
DP	6.54	-1.61	-0.50	-1.69	-0.08	-0.36	-0.37	-0.03	-0.01	0.16

rest of Pearson correlation coefficients in the Table4.3 are small which indicate that it could there exist nonlinear relationships between the human factors. Therefore, Spearman correlation (rank based) can be used to evaluate the monotonic relationship between two variables.

Spearman Correlation Test

To determine if there is a monotonic relationship between two variables of human factors, the Spearman correlation was utilized, and the results are shown in the Table 4.3. The range of the correlation coefficient (ρ) can be from -1 to 1. The $\rho = 1$ implies a perfect positive relationship and $\rho = -1$ implies a perfect negative relationship [62]. The same Cohen's standard was used here to evaluate the correlation coefficients. The Table 4.3 shows the Spearman rank correlation coefficients with p-values. It is obvious that there is no high monotonic relationship except for the same human factors that are highly correlated in terms of the Pearson correlation. Some variables have more monotonic relationships than linear relationships as seen between RT and each of GD, FD, and SV with negative moderate ρ and (p-value < 0.01).

Joint Probability Distribution of Human Factors

Joint Probability distributions can be used for the pairs of human factors that have large correlations shown in the previous section. A joint probability density function (joint PDF) will characterize the Joint Probability distribution of those two variables. Using R software, the histogram and PDF of the human factors are shown in the Figure 4.2. By considering highly correlated human factor from the Table 4.3, possible combinations with k-dependent variables can be written as

$$C1 = (SpO, SpV, VP), C2 = (GD, FD), C3 = (WV, SV)$$

and the other variables, RT, WM, and DP are uncorrelated with each of the combination C1, C2, and C3. The human factors can be rewritten in subsets as:

$$HF = \{S1, S2, S3, RT, WM, DP\}$$

where

S1= { SpO,SpV,VP }, S2={GD,FD}, S3={WV,SV}

and all these subsets are independent, so the joint probability distribution of HF will be:

$$P(HF) = P(SpO, SpV, VP)P(GD, FD)P(WV, SV)P(RT)P(WM)P(DP)$$

Table 4.3: Pearson and Spearman Correlation Tests

HF	HF	Pearson corr.			Spearman corr.		
		r	p-value	strength	ρ	p-value	strength
SpO	SpV	0.67	6.31e-13	large	0.71	3.83e-15	large
SpO	VP	0.60	6.93e-10	large	0.64	1.14e-11	large
SpV	VP	0.61	4.64e-10	large	0.59	1.20e-09	large
GD	FD	0.65	7.21e-12	large	0.62	9.08e-11	large
WV	SV	0.67	5.46e-13	large	0.73	5.73e-16	large

Table 4.3 continued from previous page

HF	HF	Pearson corr.			Spearman corr.		
		r	p-value	strength	ρ	p-value	strength
RT	SpO	-0.44	1.87e-05	medium	-0.46	5.4e-6	medium
RT	SpV	-0.46	7.12e-06	medium	-0.40	1.1e-4	medium
RT	VP	-0.39	1.45e-04	medium	-0.32	0.003	medium
RT	WM	-0.32	8.17e-05	medium	-0.36	0.001	medium
RT	WV	-0.41	1.77e-02	medium	-0.33	0.002	medium
SpO	WM	0.30	0.004	medium	0.33	0.001	medium
SpO	FD	0.32	2.57e-03	medium	0.32	0.003	medium
SpO	DP	-0.35	0.0006	medium	-0.43	2.6e-5	medium
SpV	WM	0.35	0.0007	medium	0.40	9.9e-5	medium
VP	GD	0.31	3.46e-03	medium	0.31	0.003	medium
VP	FD	0.36	5.44e-04	medium	0.33	0.002	medium
RT	GD	-0.22	0.0405	Small	-0.34	0.001	medium
RT	FD	-0.26	0.0144	Small	-0.30	0.004	medium
RT	SV	-0.25	0.0177	Small	-0.30	0.004	medium
RT	DP	0.18	0.096	Small	0.24	0.022	Small
SpO	GD	0.29	6.47e-03	Small	0.34	0.001	medium
SpO	WV	0.13	0.23	Small	0.12	0.26	Small
SpO	SV	0.02	0.86	Small	0.05	0.62	Small
SpV	GD	0.12	0.276	Small	0.19	0.08	Small
SpV	FD	0.27	0.0105	Small	0.27	0.01	Small
SpV	WV	0.05	0.64	Small	0.04	0.71	Small
SpV	SV	0.03	0.780	Small	0.04	0.68	Small

Table 4.3 continued from previous page

HF	HF	Pearson corr.			Spearman corr.		
		r	p-value	strength	ρ	p-value	strength
SpV	DP	-0.17	0.120	Small	-0.29	0.006	Small
VP	WM	0.29	0.0056	Small	0.29	0.006	Small
VP	WV	0.12	0.253	Small	0.10	0.36	Small
VP	SV	0.15	0.171	Small	0.12	0.25	Small
VP	DP	-0.20	0.06	Small	-0.29	0.006	Small
WM	GD	0.04	0.71	Small	0.08	0.43	Small
WM	FD	0.25	0.164	Small	0.28	0.007	Small
WM	WV	0.01	0.92	Small	0.04	0.72	Small
WM	SV	0.07	0.532	Small	0.08	0.53	Small
WM	DP	-0.10	0.34	Small	-0.11	0.28	Small
GD	WV	-0.9e-3	0.993	Small	0.04	0.68	Small
GD	SV	-0.01	0.90	Small	-0.008	0.98	Small
GD	DP	-0.18	0.085	Small	-0.15	0.15	Small
FD	WV	0.07	0.544	Small	0.13	0.21	Small
FD	SV	0.10	0.351	Small	0.15	0.17	Small
FD	DP	-0.12	0.26	Small	-0.10	0.34	Small
WV	DP	-0.29	0.005	Small	-0.25	0.02	Small
SV	DP	-0.07	0.48	Small	-0.11	0.29	Small
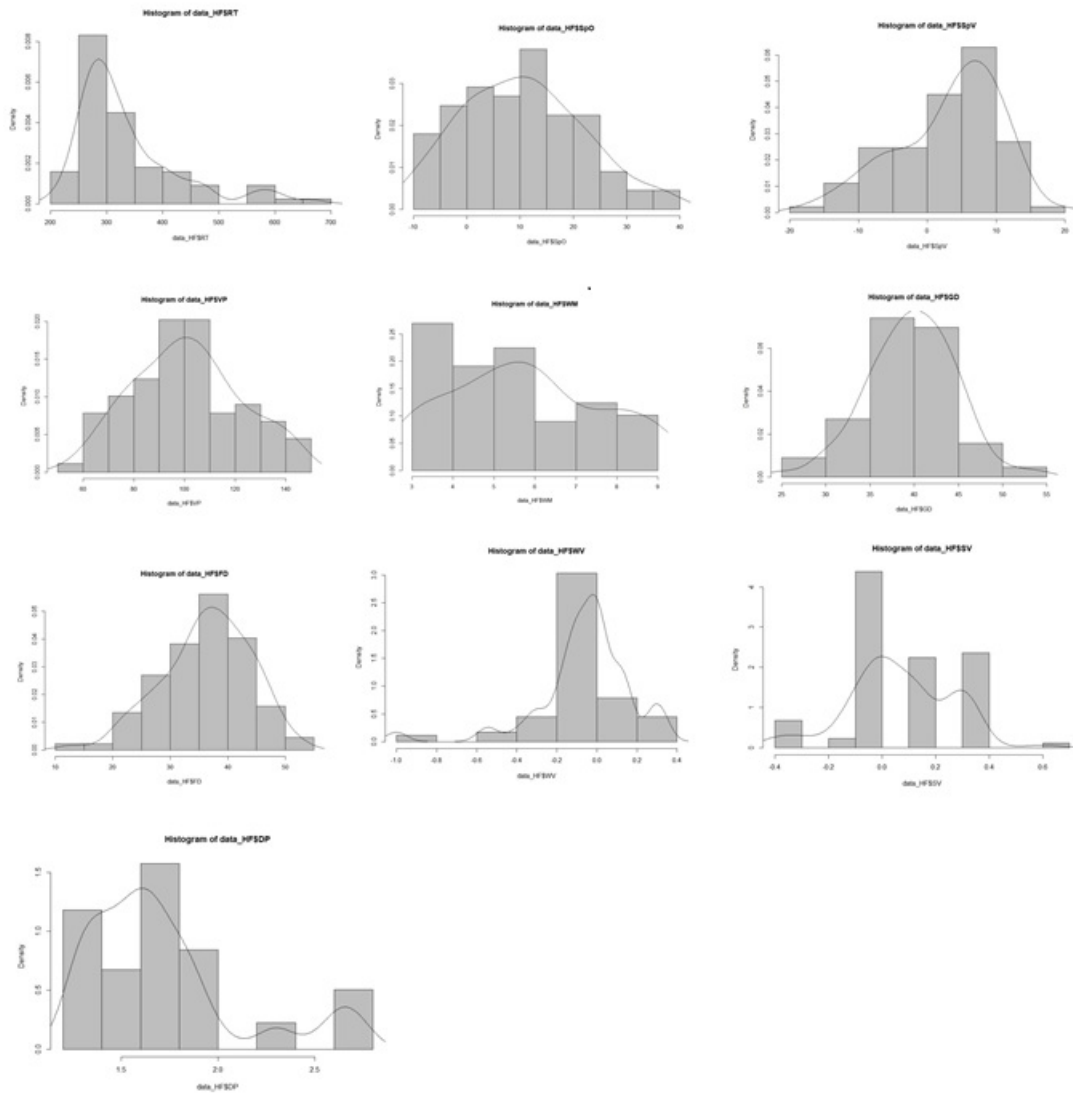
Figure 4.2: Histogram and PDF of the Human Factors

Principal Components Analysis of Human Factors

Principal Component Analysis (PCA) is an approach for reducing the dimensionality of big data sets by converting a large collection of variables into a smaller one that maintains the majority of the information in the large set [63]. For our analysis here, the principal components are linear combinations (without intercepts) of human factor variables, and the coefficients of these components are the eigenvectors of the covariance matrix of the human factors. The first principal component has the largest eigenvalue and corresponding eigenvector and is the linear combination of human factors with the greatest variance of all linear combinations. For as much of the remaining variance as possible, the second principal component is a linear combination of human factors, and so on for the other principal components as the eigenvalues are sorted descendingly. The details of finding the principal components of the human factors are in the following steps:

Step 1: Choosing a subset of principal components.

First, as human factors have different scales,for each variable, the data has been standardized by subtracting the mean first and then dividing by the standard deviation. In this case, the covariance matrix of the standardized data is identical to the correlation matrix of the unstandardized data. Following standardization, each human factor has a variance of one, and the overall variation is the sum of these variations, which in this case is 10. The eigenvalues of the correlation matrix are shown in the second column in the Table 4.4. The percentage of variance described by each of the principal components, as well as the total percentage of variation explained, are also reported in the Table 4.4. The first principal component explains 34.43% of the variation and second one explains 17.3% of the variation. The first five principal components explain 81.9% , while the first six principal components explain 87.9% of the variation. Therefore, we can select only the first six principal components to explain about 88% of the variation.

Table 4.4: Eigenvalues and the proportion of variation explained by the principal components.

Principal Component	Eigenvalue	Proportion %	Cumulative %
1	3.43	34.3	34.3
2	1.73	17.3	51.6
3	1.28	12.8	64.4
4	0.97	9.7	74.1
5	0.78	7.8	81.9
6	0.60	6.0	87.9
7	0.39	3.9	91.8
8	0.32	3.2	95.0
9	0.27	2.7	97.7
10	0.23	2.3	100

Step 2: Computing the scores of the principal component.

The principal component scores can be computed by using the eigenvectors shown in the Table 4.5. For the first principal component, it will be :

$$Y_1 = 0.374RT - 0.427SpO - 0.398SpV - 0.413VP - 0.261WM - 0.260GD - 0.320FD - 0.192WV - 0.151SV + 0.225DP$$

Step 3: Interpretation of the principal components:

Interpretation of the principal components is based on finding which human factors are most strongly ($|r| > 0.5$) correlated with each component. These larger correlations are in boldface in the Table 4.6.

PC1: the first principal component is strongly correlated with RT, SpO, SpV, VP, and FD. This suggests that these five variables vary together and therefore they are correlated.

PC2: is a measure of WV and SV as they are related positively to this component.

Table 4.5: Coefficients of Principal Components (Eigenvectors).

	PC1	PC2	PC3	PC4	PC5	PC6	PC7	PC8	PC9	PC10
RT	0.374	-0.183	0.106	-0.165	0.024	-0.793	0.209	-0.144	0.087	0.294
SpO	-0.427	-0.146	-0.191	-0.242	-0.157	-0.027	0.315	-0.659	0.238	-0.291
SpV	-0.398	-0.163	-0.368	0.023	-0.255	-0.052	0.416	0.327	-0.400	0.414
VP	-0.413	-0.111	-0.110	0.026	-0.323	-0.394	-0.674	0.184	0.237	-0.029
WM	-0.261	-0.095	-0.279	0.383	0.781	-0.132	-0.115	-0.177	0.003	0.164
GD	-0.260	-0.223	0.652	-0.017	-0.040	0.129	-0.206	-0.355	-0.358	0.377
FD	-0.320	-0.182	0.526	0.244	0.124	-0.117	0.396	0.406	0.327	-0.266
WV	-0.192	0.649	0.088	-0.058	-0.024	0.068	0.099	-0.040	0.475	0.538
SV	-0.151	0.614	0.111	0.257	-0.075	-0.392	0.060	-0.127	-0.478	-0.337
DP	0.225	-0.129	-0.064	0.798	-0.416	0.075	0.066	-0.254	0.174	0.119

Table 4.6: Correlation Coefficients between the Principal Component Scores and Human Factors

	PC1	PC2	PC3	PC4	PC5	PC6	PC7	PC8	PC9	PC10
RT	0.69	-0.24	0.12	-0.16	0.02	-0.61	0.13	-0.08	0.05	0.14
SpO	-0.79	-0.19	-0.22	-0.24	-0.14	-0.02	0.20	-0.37	0.12	-0.14
SpV	-0.74	-0.21	-0.42	0.02	-0.23	-0.04	0.26	0.19	-0.21	0.20
VP	-0.77	-0.15	-0.12	0.03	-0.28	-0.30	-0.42	0.10	0.12	-0.01
WM	-0.48	-0.13	-0.32	0.38	0.69	-0.10	-0.07	-0.10	0.00	0.08
GD	-0.48	-0.29	0.74	-0.02	-0.03	0.10	-0.13	-0.20	-0.19	0.18
FD	-0.59	-0.24	0.60	0.24	0.11	-0.09	0.25	0.23	0.17	-0.13
WV	-0.36	0.85	0.10	-0.06	-0.02	0.05	0.06	-0.02	0.25	0.26
SV	-0.28	0.81	0.13	0.25	-0.07	-0.30	0.04	-0.07	-0.25	-0.16
DP	0.42	-0.17	-0.07	0.79	-0.37	0.06	0.04	-0.14	0.09	0.06

PC3: is strongly correlated with the dexterity measures (FD and FD) .

PC4: is strongly correlated with DP.

PC5: is strongly correlated with WM.

Step4: Using Varimax Rotation to rotate selected PCs of the Human Factors:

To get clear interpretations of the principal components, a varimax rotation can be utilized to

transform the selected principal components to other orthogonal subsets. Because the data are standardized to have a variance of one, the relative magnitude of each coefficient of the PC can be directly assessed to give a measure of how each variable contribute to that PC. The Table 4.7 shows the rotated PCs and that :

PC1 is associated with SpO, SpV, and VP and this component is a measure of these variables.

PC2 is associated with WV and SV.

PC3 is associated with GD and FD.

PC4 is associated with DP.

PC5 is associated with WM.

PC6 is associated with RT.

Therefore, these principal components represent orthogonal subspaces of human factors and they can be written as:

$$HF = \{\{SpO, SpV, VP\}, \{WV, SV\}, \{GD, FD\}, RT, WM, DP\}$$

The correlations between the scores of rotated principal components and the human factors were tested as shown in the Table 4.8. The results coincide with the contributions of the coefficients of the human factors to the PCs shown in the Table 4.7

Table 4.7: Coefficients of rotated Principal Components PC1-PC6

	PC1	PC2	PC3	PC4	PC5	PC6
RT	0.050	0.034	-0.030	0.056	0.028	0.913
SpO	-0.515	0.074	0.011	0.208	0.039	-0.093
SpV	-0.595	0.059	-0.106	-0.084	-0.047	-0.105
VP	-0.610	-0.136	0.105	-0.083	0.024	0.216
WM	0.012	0.017	0.009	0.030	-0.963	-0.028
GD	0.035	0.078	0.717	0.075	0.166	-0.087
FD	-0.020	-0.061	0.679	-0.069	-0.165	0.063
WV	0.060	-0.609	-0.043	0.175	0.091	-0.243
SV	-0.027	-0.768	0.026	-0.127	-0.065	0.161
DP	0.015	0.026	-0.002	-0.939	0.032	-0.055

Table 4.8: Correlation Coefficients between the Human Factors and the Scores of Rotated Principal Components.

	PC1	PC2	PC3	PC4	PC5	PC6
RT	0.26	0.36	-0.27	-0.17	0.31	0.97
SpO	-0.86	-0.06	0.33	0.42	-0.28	-0.45
SpV	-0.88	-0.04	0.19	0.14	-0.38	-0.45
VP	-0.86	-0.20	0.40	0.16	-0.28	-0.27
WM	-0.37	-0.05	0.17	0.09	-0.99	-0.29
GD	-0.26	0.02	0.91	0.21	0.02	-0.21
FD	-0.37	-0.11	0.90	0.09	-0.30	-0.21
WV	-0.10	-0.89	0.03	0.33	0.01	-0.47
SV	-0.08	-0.93	0.06	0.03	-0.09	-0.19
DP	0.27	0.19	-0.17	-0.98	0.09	0.18

CHAPTER 5: CONCLUSION AND FUTURE WORK

In Chapter Two, an intelligent adaptive grasping algorithm for novel objects has been implemented relying on slip velocity and gripper force measurements. A two-finger robot gripper prototype was embedded with a laser sensor extracted from a Mouse device for slippage measurement. Also, it was embedded with FSR sensor for force measurement. Analysis shows that the adaptive controller can estimate the exact minimal grasping force for the fully filled bottle and with 0.2 N force error for the half-filled bottle. Simulation and experimental results both show that this method can immobilize a novel object within the fingers of the gripper with minimal deformation. Compared with a previously designed adaptive grasping algorithm in [19], this algorithm design reduces controller complexity; however, it yields similar performance.

To generalize our work for both translational and rotational slipping avoidance, a novel real-time switching-control based adaptive grasping algorithm to control grasping force application by a standard robotic gripper was presented in Chapter Three. In addition, we presented the design and a prototype of a two-finger sensorized robotic gripper embedded with force sensor (FSR) and two slip sensors for translational and rotational slip velocity measurements. Experimental data collected from using objects with different sizes and shapes show that the algorithm applies close to the minimal force needed to safely grasp objects by preventing both linear and angular slippage with force deviation percentage $(3.80\% - 5.49\%)$ for predominantly translational slipping case, and $(2.27\% - 7.50\%)$ for predominantly rotational slipping case without excessive deformation seen. Also, the experimental results show that the controller prevents successfully the translational and rotational slippage for non-flat objects and for hand configurations not aligned with the axis of gravity. Furthermore, experimental results using the UCF-MANUS robotic system illustrate that the algorithm is robust, safe, and computationally efficient. It is easy to see that the prototype and algorithm are simple and low-cost (about $150 for FSR, two slip sensors, and adapter) to add

intelligent and adaptive force application ability to any standard gripper.

In Chapter Four, using experiment data collected from recruiting 93 participants, dependency analysis of human factors was presented utilizing the Pearson and Spearman correlation tests to capture the joint probability distribution of human factors. The results have shown that the following human factors were jointly distributed within the same set: (spatial visualization (SpV), spatial orientation (SpO), and visual perception (VP)), (gross dexterity (GD) and fine dexterity (FD)) and (visual acuity WV and SV). On the other hand, it was found weak correlations (i.e. no joint distribution) between the Reaction Time (RT), working memory (WM), depth perception (DP) and between these variables and those in groups above. Also, the Principal Components Analysis (PCA) of human factors reported the same observations regarding the dependencies between the human factors. Based on this model of joint probability distribution, one can build a probabilistic model to infer user parameters and then compensate for any deficit in human factors during operating an assistive robot which in turn can improve the grasping activities and reduce object slippage possibilities.

Our future work will indeed focus on a sensorless formulation by utilizing a gripper embedded pressure sensor grid in lieu of the combination of two slip sensors and an FSR used here. It can be extended for three- or four- finger gripper robotic arm. Also, the algorithm can be developed to fit in-hand manipulation tasks especially those needed controlled rotational sliding of objects.

LIST OF REFERENCES

[1] H. Sani and S. Meek, "Characterizing the performance of an optical slip sensor for grip control in a prosthesis," in *Proc. IEEE/RSJ Int. Conf. Intell. Robots Syst.*, pp. 1927–1932, Sep. 2011.

[2] L. Roberts, G. Singhal, and R. Kaliki, "Slip detection and grip adjustment using optical tracking in prosthetic hands," *2011 Annual International Conference of the IEEE Engineering in Medicine and Biology Society*, 2011.

[3] M. Saen, K. Ito, and K. Osada , "Action-Intention-Based Grasp Control With Fine Finger-Force Adjustment Using Combined Optical-Mechanical Tactile Sensor," *IEEE Sensors Journal*, vol. 14, no.11, pp. 4026-4033, Nov. 2014

[4] H. Hasegawa, Y. Mizoguchi, K. Tadakuma, A. Ming, M. Ishikawa, and M. Shimojo, "Development of intelligent robot hand using proximity, contact and slip sensing," in *Proc. IEEE Int. Conf. Robot. Autom.*, May 2010, pp. 777–784.

[5] D. Gunji, T. Araki, A. Namiki, A. Ming, and M. Shimojo, "Grasping force control of multi-fingered robot hand based on slip detection using tactile sensor," *Journal of the Robotics Society of Japan*, vol. 25, no. 6, pp. 970-978, 2007.

[6] S. Teshigawara, T. Tsutsumi, S. Shimizu, Y. Suzuki, A. Ming, M. Ishikawa, and M. Shimojo, "Highly Sensitive Sensor for Detection of Initial Slip and Its Application in a Multi-fingered Robot Hand," *Proc. IEEE Int. Conf. on Robotics and Automation*, pp.1097-1102, 2011.

[7] E. Engeberg and S. Meek, "Adaptive sliding mode control for prosthetic hands to simultaneously prevent slip and minimize deformation of grasped objects," *IEEE/ASME Trans. Mechatronics*, vol. 18, no. 1, pp. 376-385, Feb. 2013.

[8] Zhe Su, K. Hausman, Y. Chebotar, A. Molchanov, G.E. Loeb, G.S. Sukhatme, and S. Schaal, "Force estimation and slip detection/classification for grip control using a biomimetic tactile sensor," in *2015 IEEE-RAS 15th International Conference on Humanoid Robots (Humanoids)*, pp. 297-303, 2015.

[9] Cirillo, A., Cirillo, P., De Maria, G., Natale, C., Pirozzi, S., "Control of linear and rotational slippage based on six-axis force/tactile sensor," *Proceedings - IEEE International Conference on Robotics and Automation*, art. no. 7989188, pp. 1587-1594, 2017.

[10] Costanzo, M., De Maria, G., Natale, C., "Slipping Control Algorithms for Object Manipulation with Sensorized Parallel Grippers," *Proceedings - IEEE International Conference on Robotics and Automation*, art. no. 8460883, pp. 7455-7461, 2018.

[11] Costanzo, M., Stelter, S., Natale, C., Pirozzi, S., Bartels, G., Maldonado, A., Beetz, M., "Manipulation Planning and Control for Shelf Replenishment," *IEEE Robotics and Automation Letters*, 5 (2), art. no. 8968346, pp. 1595-1601, 2020.

[12] J.M. Romano, K. Hsiao,G. Niemeyer, S. Chitta, and K.J. Kuchenbecker, "Human-Inspired Robotic Grasp Control With Tactile Sensing," *IEEE Transactions on Robotics*, 27(6), pp. 1067-1079, 2011.

[13] F. Veiga , J. Peters , and T. Hermans, "Grip Stabilization of Novel Objects using Slip Prediction," *IEEE Transactions on Haptics*, 11(4), pp. 531-542, 2018.

[14] F. Veiga, B. Edin, and J. Peters, "Grip stabilization through independent finger tactile feedback control," *MDPI Sensors*, 20, 1748; doi:10.3390/s20061748, 2020.

[15] B. Sundarlingam, S. Lambert, A. Handa, B. Boots, T. Hermans, S. Birchfield, N. Ratliff, D. Fox, "Robust Learning of Tactile Force Estimation through Robot Interaction", *IEEE ICRA,* May 2019.

[16] B. Sundarlingam and T. Hermans, "In-Hand Object-Dynamics Inference using Tactile Fingertips," *IEEE Transactions on Robotics*, 37(4), pp. 1115-1126, 2021.

[17] T. N. Le, F. Verdoja, F. J. Abu-Dakka, and V. Kyrki, "Probabilistic Surface Friction Estimation Based on Visual and Haptic Measurements " *IEEE Robotics and Automation Letters*,vol. 6, no. 2, pp. 2838-2845, April 2021, doi: 10.1109/LRA.2021.3062585.

[18] D.-J. Kim, Z. Wang, and A. Behal, "Motion Segmentation and Control Design for UCF-MANUS - An Intelligent Assistive Robotic Manipulator," *IEEE/ASME Transactions on Mechatronics*, vol. 17, no. 5, pp. 936-948, Sep. 2012.

[19] Z. Ding, N. Paperno, K. Prakash, and A. Behal, "An Adaptive Control Based Approach for 1-Click Gripping of Novel Objects using a Robotic Manipulator," *IEEE Transactions on Control Systems Technology*, vol. 27, no. 4, pp. 1805-1812, July 2019, doi: 10.1109/TCST.2018.2821651.

[20] M. Al-Mohammed and Z. Ding and P. Liu and A. Behal "An Adaptive Control Based Approach for Gripping Novel Objects with Minimal Grasping Force," *IEEE 14th International Conference on Control and Automation (ICCA) Anchorage, AK, 2018,*, pp.1040-1045.

[21] M. Al-Mohammed, R. Adem, and A. Behal "A Switched Adaptive Controller for Robotic Gripping of Novel Objects with Minimal Force," *IEEE Transactions on Control Systems Technology*, accepted, 2022.

[22] C. Lathan and M. Tracey, "The Effects of Operator Spatial Perception and Sensory Feedback on Human-Robot Teleoperation Performance," *Presence: Teleoperators and Virtual Environments*, vol. 11, no. 4, pp. 368-377, August 2002.

[23] J. Gomer and C. Pagano, "Spatial Perception and Robot Operation: Should Spatial Abilities Be Considered When Selecting Robot Operators?," *Proceedings of the Human Factors and Ergonomics Society Annual Meeting*, vol. 55, no. 1, pp. 1260-1264, September 2011.

[24] L. Long et al, "Investigating the Relationship between Visual Spatial Abilities and Robot Operation during Direct Line of Sight and Teleoperation," *Proceedings of the Human 8 Factors and Ergonomics Society Annual Meeting*, vol. 53, no. 18, pp. 1437-1441, October 2009.

[25] L.O. Long et al, "Visual Spatial Abilities in Uninhabited Ground Vehicle Task Performance During Teleoperation and Direct Line of Sight," *Presence: Teleoperators and Virtual Environments,* vol. 20, no. 5, pp. 466-479, October 2011.

[26] M. E. Morphew et al, "Human Performance in Space". *Ergonomics in Design: The Quarterly of Human Factors Applications,* vol. 9 no. 4, 6-11, October 2001

[27] C. Wang et al, "Predicting Performance in Manually Controlled Rendezvous and Docking Through Spatial Abilities," *Advances in Space Research,* vol. 53, no. 2, pp. 362-369, January 2014.

[28] M. Menchaca-Brandan et al, "Influence of Perspective-taking and Mental Rotation Abilities in Space Teleoperation," in *2nd ACM/IEEE International Conference on Human-Robot Interaction (HRI),* March 2007, pp. 271-278.

[29] N. Paperno, M. Rupp, E. M. Maboudou-Tchao, J. A. Smither and A. Behal., "A Predictive Model for Use of an Assistive Robotic Manipulator: Human Factors Versus Performance in Pick-and- Place/Retrieval Tasks," in *IEEE Transactions on Human-Machine Systems*, vol. 46, no. 6, pp. 846-858, December 2016

[30] Salthouse, Timothy A., et al. "Interrelations of age, visual acuity, and cognitive functioning," *The Journals of Gerontology Series B: Psychological Sciences and Social Sciences*, 51.6 (1996): P317-330.

[31] Kim, Dae-Jin, et al."How autonomy impacts performance and satisfaction: Results from a study with spinal cord injured subjects using an assistive robot," *IEEE Transactions on Systems, Man, and Cybernetics-Part A: Systems and Humans* ,42.1 (2011): 2-14.

[32] Chung, Cheng-Shiu, Hongwu Wang, and Rory A. Cooper. "Functional assessment and performance evaluation for assistive robotic manipulators: Literature review." The journal of spinal cord medicine 36.4 (2013): 273-289.

[33] N. Bevan et al.,"What is usability,"presented at the 4th Int. *Conf. Human- Comput. Interact.*, Stuttgart, Germany, Sep. 1991.

[34] Leo Breiman. Random forests. Machine learning 45, no. 1 (2001): 5-32.

[35] Mendenhall, William M., and Terry L. Sincich. Statistics for Engineering and the Sciences. Chapman and Hall/CRC, 2016.

[36] D.-J. Kim, Z. Wang, N. Paperno, and A. Behal, "System Design and Implementation of UCF-MANUS—An Intelligent Assistive Robotic Manipulator," in *IEEE/ASME Transactions on Mechatronics*, vol.19, no.1, pp.225-237, Feb. 2014.

[37] A. Behal, W. E. Dixon, D. M. Dawson, and B. Xian, *Lyapunov-Based Control of Robotic Systems*, CRC Press, December 17, 2009, ISBN 0-8493-7025-6.

[38] J.J.E. Slotine and W. Li, Applied Nonlinear Control, Prentice Hall, Inc: Englewood Cliffs, NJ, 1991.

[39] online, `https://www.interlinkelectronics.com/fsr-400-series`

[40] online, https://www.logitech.com/

[41] A. L. Fetter, J. D. Walecka, *Theoretical Mechanics of Particles and Continua*. Milenola , New York, USA: Dover Publications, INC., 2003.

[42] online, `https://www.tekscan.com/products-solutions/`
`force-sensors/a201`

[43] UCF Assistive Robotics Lab, Multimedia, online, `https://www.ece.ucf.edu/`
`abehal/AssistiveRobotics/multimedia.php`

[44] D.-J. Kim et al, "On the Relationship between Autonomy, Performance, and Satisfaction: Lessons from a Three Week User Study with post- SCI Patients using a Smart 6DOF Assistive Robotic Manipulator," 2010 *IEEE International Conference on Robotics and Automation*, May 2010, pp. 217-222,

[45] D. J. Kim et al., "System Design and Implementation of UCFMANUS— an Intelligent Assistive Robotic Manipulator," *IEEE/ASME Transactions on Mechatronics,* vol. 19, no. 1, 225-237, February 2014.

[46] D.-J. Kim et al., "A Region-based Switching Scheme for Practical Visual Servoing under Limited FOV and Dynamically Changing Features," presented at *the IASTED 14th Int. Conf. Robotic Applications,* November 2009.

[47] K. Schneider. *Matlab and Psychophsics Toolbox Seminar, Part 3:Timing and Input*. August 2006, www.yorku.ca/keiths/ptb/part3.pdf.

[48] Birte U. Forstmann, Marc Tittgemeyer, et al., "The Speed-Accuracy Tradeoff in the Elderly Brain: A Structural Model-Based Approach,"*Journal of Neuroscience 23 November,* 2011, 31 (47) 17242-17249; DOI: 10.1523/JNEUROSCI.0309-11.2011

[49] Perri, Rinaldo Livio et al. "Individual differences in response speed and accuracy are associated to specific brain activities of two interacting systems." *Frontiers in behavioral neuroscience,* vol. 8 251. 22 Jul. 2014, doi:10.3389/fnbeh.2014.00251

[50] S. Thompson et al, "Kinematic Analysis of Multiple Constraints on a Pointing Task," *Human Movement Science*, vol. 26, no. 1, pp. 11-26, February 2007.

[51] R. Ekstrom et al., *Kit of Factor-Referenced Cognitive Tests*. Princeton, NJ: Educational Testing Service (ETS), August 1976.

[52] R. Colarusso and D. Hammill, *Motor-Free Visual Perception Test*. San Rafael, Calif.: Academic Therapy Pub., 1972.

[53] R.A. Stern and T. White, *NAB Digits Forward/Backward Test*. Psychological Assessment Resources, Inc.

[54] G. Miller, "The Magical Number Seven, Plus or Minus Two: Some Limits on Our Capacity for Processing Information.," *Psychological Review,* vol. 63, no. 2, pp. 81-97, March 1956.

[55] J. Tiffin and E. Asher, "The Purdue Pegboard: Norms and Studies of Reliability and Validity," Journal of Applied Psychology, vol. 32, no. 3, pp. 234-247, June 1948.

[56] Lowvision.preventblindness.org, "Low Vision Resources Center — How Visual Acuity Is Measured," http://lowvision.preventblindness.org/eyeconditions/ how-visual-acuity-is-measured, 2003.

[57] *Randot Stereotests*, Stereo Optical Co., Inc.

[58] I. Laffont et al., "Evaluation of a Graphic Interface to Control A Robotic Grasping Arm: A Multicenter Study, " *Archives of Physical Medicine and Rehabilitation,* vol. 90, no. 10, pp. 1740-1748, October 2009.

[59] C. A. Smarr et al., "Domestic robots for older adults: attitudes, preferences, and potential," *International Journal of Social Robotics*, vol. 6, no. 2, pp. 229-247, 2014.

[60] Edwards, A. L. *An Introduction to Linear Regression and Correlation.* San Francisco, CA: W. H. Freeman, 1976.

[61] "SPSS Tutorials: Pearson Correlation" `https://libguides.library.kent.edu/SPSS/PearsonCorr`

[62] Rees, D.G. *Essential Statistics*. Chapman and Hall/CRC, 2000.

[63] Jolliffe, I. T. *Principal Component Analysis*. Springer Series in Statistics. New York: Springer-Verlag, 2002.